Nonequilibrium Theory of the Conversion Efficiency Limit of Solar Cells Including Thermalization and Extraction of Carriers

Kenji Kamide,[1,*] Toshimitsu Mochizuki,[1] Hidefumi Akiyama,[2,3] and Hidetaka Takato[1]

[1] *Renewable Energy Research Center, National Institute of Advanced Industrial Science and Technology (AIST), Koriyama, Fukushima 963-0298, Japan*

[2] *The Institute for Solid State Physics (ISSP), The University of Tokyo, Kashiwa, Chiba 277-8581, Japan*

[3] *OPERANDO-OIL, Kashiwa, Chiba, 277-8581, Japan*

The ideal solar-cell conversion efficiency limit known as the Shockley-Queisser (SQ) limit, which is based on a detailed balance between absorption and radiation, has long been a target for solar-cell researchers. While the theory for this limit uses several assumptions, the requirements in real devices have not been discussed fully. Given the current situation in which research-level cell efficiencies are approaching the SQ limit, a quantitative argument with regard to these requirements is worthwhile in terms of the understanding of the remaining loss mechanisms in current devices and the device characteristics of solar cells that are operating outside the detailed balance conditions. Here we examine two basic assumptions: (1) that the photogenerated carriers lose their kinetic energy via phonon emission in a moment (fast thermalization), and (2) that the photogenerated carriers are extracted into carrier reservoirs in a moment (fast extraction). Using a model that accounts for the carrier relaxation and extraction dynamics, we reformulate the nonequilibrium theory for solar cells in a manner that covers both the equilibrium and nonequilibrium regimes. Using a simple planar solar cell as an example, we address the parameter regime in terms of the carrier extraction time and then consider where the conventional SQ theory applies and what could happen outside the applicable range.

I. INTRODUCTION

Shockley and Queisser (SQ) determined a theoretical estimate for the upper limit of the conversion efficiency in an ideal solar cell [1]. The original SQ theory takes radiative recombination into account as a main cause of the current loss in solar cells in a simple manner. The energy distributions of the carriers, denoted by $n_{E_e}^e$ for electrons and $n_{E_h}^h$ for holes, must be known to evaluate the radiative recombination rate because it is proportional to the sum of their product. SQ theory assumes that the carriers in the absorber are in thermal and chemical equilibrium with both the lattice phonons and the carriers in the electrodes at an ambient temperature T_c and with chemical potentials of μ_c for the conduction electrons and μ_v for the valence electrons. The resulting current-voltage relationship given by $I = I(V) = I_{\text{sun}} + I_{\text{rad}}^0(1 - e^{|e|V/k_B T_c})$, where the voltage between the electrodes is equal to the Fermi level separation within the absorber, $|e|V = \mu_c - \mu_v$, ultimately determines the conversion efficiency during maximum power operation, where I_{sun} is the photogenerated current produced by absorption of sunlight. The theoretical

efficiency limit has been refined by including various factors (e.g., Auger recombination, light trapping, photon recycling, and Coulomb interactions [2]) under the detailed balance assumption, and seems to have given a reasonable estimate as far as seeing the timeline of the best research solar-cell efficiencies [provided by the National Renewable Energy Laboratory (NREL)]. However, the basic assumption could require reconsideration in some cases, as discussed below.

The requirements for the assumptions used in the SQ theory to be justified are commonly described as follows:

(1) the photogenerated carriers lose their kinetic energy via phonon emission and rapidly establish their thermal equilibrium distribution in a moment (which is called fast thermalization);

(2) the carriers are extracted rapidly into carrier reservoirs immediately after they are produced (which is called fast extraction).

The latter assumption (2) is actually given explicitly in the original paper [1]. However, the above requirements are not sufficiently clear and thus some quantitative issues

---

*kenji.kamide@aist.go.jp

remain. While the two time scales, i.e., the carrier thermalization time, τ_{ph}, and the carrier extraction time, τ_{out}, are assumed to be short, the following questions are not addressed: first, how short should these times be, i.e., which time scales from other processes should be compared with these times, and second, how do τ_{ph} and τ_{out} compare? The latter question relates directly to the concept of hot carrier solar cells operating out of equilibrium [3–7], where fast carrier extraction before the thermalization is complete can reduce the thermalization losses and ensure that device performance is not limited by a detailed balance.

Record efficiencies of recent cell research are gradually approaching the SQ limits in nonconcentrator-type single-junction solar cells, e.g., Kaneka's Si-based cell with 26.7% efficiency and Alta Devices' thin-film GaAs-based cell with 28.8% efficiency [8]. It is, therefore, important to have a more precise understanding of the situation in which detailed balance theory provides a reliable estimate of the attainable upper efficiency limit. Quantitative estimation of the parameters to which the SQ theory applies will help to clarify the remaining energy losses and push current device performance towards the SQ limit. Additionally, a more precise understanding of the energy-conversion mechanisms outside the detailed balance condition will lead to new strategies for future improvements that are intended to go beyond the SQ limit.

The nonequilibrium dynamics of many particle systems can be described in general terms using nonequilibrium Green functions (NEGFs) [9–11]. These functions were initially applied to study electron transport in solids and in mesoscopic devices [12,13], and later in semiconductor light-emitting devices (e.g., light-emitting diodes or LEDs [14], semiconductor lasers [15], quantum cascade lasers [16], and polariton condensates [17,18]). More recently, the NEGF formalism was also used to study solar cells, mostly applied to nanostructured solar cells [19–21], where the device characteristics are likely to be affected strongly by the quantum transport of carriers whose dynamics should be studied with the spacial resolution. NEGFs were also used to study the conditions required to validate use of luminescence-based characterization of solar cells [22], which is justifiable in terms of photovoltaic reciprocity under the detailed balance principle [23,24]. Despite the sound theoretical basis that is available, the device characteristics have not been explored for a sufficiently wide range of parameters via the NEGF approach, particularly for solar cells. This seems to be related to the complexity of the theory and high computational costs, especially for nanostructured solar cells. Similar issues were found with an *ab initio* approach [25]

In order to answer the questions raised above, the simplest way is to incorporate the time scales τ_{out} and τ_{ph} in the theory while keeping the other settings the same as the original SQ theory. This can also be done by

applying standard theory for open systems based on the density matrix equations. In this work, we formulate such a nonequilibrium theory that does not assume any form for the distribution functions used for the carriers in the absorber, in a manner similar to the NEGF formulation. The carrier distribution functions in the absorber are determined using a set of rate equations that is derived from second-order perturbation theory based on the coupling between the absorber carriers and three baths (the phonon, electron, and hole reservoirs). Spectral broadening of the microscopic states of the carriers is also included in the relevant cases. As a result, the theory describes solar-cell operation for a wide range of parameters, including the situations where the photogenerated carriers are either in or out of thermal equilibrium.

This paper is organized as follows. In Sec. II, we formulate a nonequilibrium theory for solar cells based on the model shown in Fig. 1, and derive a set of rate equations for the microscopic carrier distribution function in the absorber. The microscopic carrier distribution function is then determined as a steady-state solution to the rate equation. At the end of this section, general expressions are given for the total output current and the total output power to enable simulation of the solar-cell device performance. In Sec. III, the basic properties required by the solution to the set of rate equations are presented before the numerical analysis begins. These properties are useful when verifying the accuracy of the simulation. Classification of the parameter regime, specifically in terms of the carrier extraction time τ_{out}, is also presented in Sec. III. Before the set of
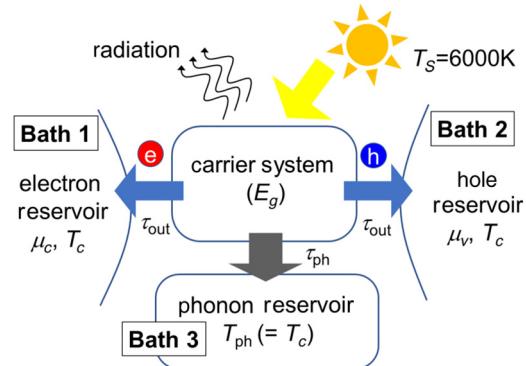

FIG. 1. Nonequilibrium model of the solar cell: electron and hole carriers in a semiconductor absorber (energy gap, E_g) interact with the carriers in the carrier reservoirs (bath 1 and bath 2) and the lattice phonons in the absorber (bath 3). Population distributions of the carriers and phonons in the three reservoirs are given using the thermal equilibrium distribution function (Fermi-Dirac distribution with chemical potentials of μ_c and μ_v for conduction and valence electrons, respectively, at temperature T_c (= 300 K), and Bose-Einstein distribution for phonons at lattice temperature T_{ph} (= T_c)). Electron-hole pairs are generated in the absorber by solar illumination (a blackbody spectrum at temperature T_S (= 6000 K) is assumed here), and the output current loss is due to radiative recombination in the absorber.

equations is solved, the equations themselves can be used to indicate the parameter regime where the assumptions of the SQ theory fail. In Sec. IV, a device performance simulation based on our formulation is presented for a simple planar single-junction solar cell. The numerical simulations show what physically happens in the photovoltaic energy-conversion processes in each of the regimes that are classified in Sec. III. In Sec. V, we summarize these findings and discuss future issues and future applications of the nonequilibrium theory.

II. NONEQUILIBRIUM THEORY (FORMULATION)

In this section, we formulate the nonequilibrium theory for solar cells. Our theory is based on the second-order perturbation theory in terms of the coupling between the absorber carriers and three baths (the phonon, electron, and hole reservoirs shown in Fig. 1). At this approximation level, as we will see in the following subsections, we can derive a set of rate equations in a closed form (the equations will not be closed for a model with carrier-carrier interaction) within the microscopic distribution functions for the electrons (e) and holes (h) in the absorber, ($\{n_{E_e}^e, n_{E_h}^h\}$):

$$\frac{d}{dt} n_{E_e}^e = R_{E_e}^{e,\text{sun}} - R_{E_e}^{e,\text{rad}} - R_{E_e}^{e,\text{out}} - R_{E_e}^{e,\text{phonon}}, \quad (1)$$

$$\frac{d}{dt} n_{E_h}^h = R_{E_h}^{h,\text{sun}} - R_{E_h}^{h,\text{rad}} - R_{E_h}^{h,\text{out}} - R_{E_h}^{h,\text{phonon}}. \quad (2)$$

Here, E_e and E_h are the carrier kinetic energies measured from the bottom of the bands (Fig. 2). The first term, $R_{E_{e(h)}}^{e(h),\text{sun}}$, on the right-hand side of the rate equations represents the carrier generation rate due to sunlight absorption. The second term, $R_{E_{e(h)}}^{e,\text{rad}}$, represents the carrier loss rate due to radiative carrier recombination. The third term, $R_{E_{e(h)}}^{e(h),\text{out}}$, represents the rate of carrier extraction to the electrodes. The last term, $R_{E_{e(h)}}^{e(h),\text{phonon}}$, represents the rate of electron scattering to other microscopic states within the same band due to phonon emission or absorption.
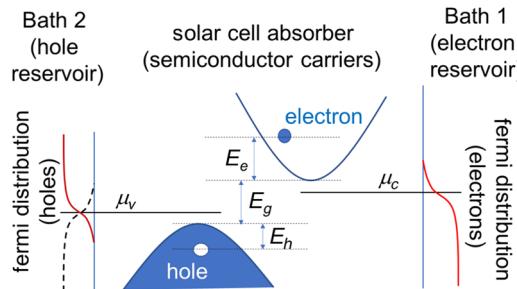
In finding the first two terms, $R_{E_{e(h)}}^{e(h),\text{sun}}$ and $R_{E_{e(h)}}^{e,\text{rad}}$, the light-matter coupling is taken into account within the second-order perturbation theory. Therefore, in this theory, the presence of the fourth bath for the radiation field (photon reservoirs and photon injection from the sun) is implicitly assumed. Therefore, we find the well-known expression for the radiation rate and the absorption coefficient in Eqs. (12) and (16). Using them, the balance between the absorption and radiation inside the absorber is incorporated through the continuity equation for the photon current [Eq. (17)]. A set of this theoretical treatment gives the net radiation loss rate, which is consistent with the generalized Planck law (see Secs. II B).

For the simulation of the solar-cell device characteristics, this equation will be solved under the steady-state condition:

$$\frac{d}{dt} n_{E_e}^e = \frac{d}{dt} n_{E_h}^h = 0. \quad (3)$$

In the following subsections, we will derive explicit expressions for $R_{E_{e(h)}}^{e(h),\text{sun}}$, $R_{E_{e(h)}}^{e(h),\text{rad}}$, $R_{E_{e(h)}}^{e(h),\text{out}}$, and $R_{E_{e(h)}}^{e(h),\text{phonon}}$ via microscopic modeling of the carriers in the simple planar solar cell (thickness w, surface area $\mathcal{A}$, volume $\mathcal{V} = \mathcal{A}w$) shown in Fig. 3.

The assumptions that were made in the original SQ model [1] are also used here to simplify the discussion but will not alter the main conclusion of this paper. For example, we consider the absorber thickness w to be larger than the absorption length but less than the minority carrier diffusion length. This allows us to consider perfect absorption of sunlight above the absorption edge ($E > E_g$) and a homogeneous carrier distribution in the absorber. Perfect antireflection behavior at the front surface, perfect passivation with zero surface recombination, and perfect carrier selectivity for contacts (this can be made by doping in front of contacts [26]) are also assumed here.

An additional simplification is made in this work to the band structure of the carriers in the absorber. An

FIG. 2. Energy diagrams for carriers in the absorber and Fermi distribution functions in the carrier reservoirs (baths 1 and 2).
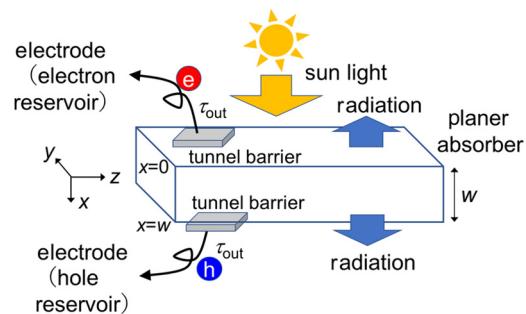
FIG. 3. Simple planar solar-cell model: a planar absorber of thickness w is illuminated by sunlight from the normal direction and photogenerated carriers are extracted to the two electrodes (baths 1 and 2) through tunneling contact. The photocarrier losses are due to radiative recombination.

effective two-band model is used to describe the microscopic carrier states under an effective-mass approximation (with infinite bandwidths), in which the effective masses for the electrons (m_e^*) and holes (m_h^*) are selected to reproduce the densities of states near the band extrema [Si: $m_e^*/m_e = (\nu_{\text{valley}}^2 m_\perp^2 m_\parallel)^{1/3}/m_e = 1.08$, $m_h^*/m_e = (m_{hh}^{3/2} + m_{lh}^{3/2})^{2/3}/m_e = 0.55$ with $\nu_{\text{valley}} = 6$, $m_\perp/m_e = 0.19$, $m_\parallel/m_e = 0.98$, $m_{hh}/m_e = 0.49$, $m_{lh}/m_e = 0.16$ with bare electron mass m_e]. Therefore, the effective masses and a single band gap E_g (1.12 eV for Si and 1.42 eV for GaAs) are the only parameters that characterize the band structure. On the other hand, the effects of the band anisotropy, the valley degree of freedom within the degenerate bands (particularly in Si), and the contributions from other bands located away from the extrema are not taken into account correctly. In this sense, our analysis is far from but is not intended to be quantitatively accurate in simulations for specific systems, but is rather intended to produce a general picture on the main issue, i.e., nonequilibrium aspects of solar cells. However, inclusion of the exact band structures away from the band edge will not change the result largely under the assumption of perfect absorption in the absorber, since the energy distributions of carriers are populated mainly near the band edge in the whole range of parameters, as will be shown in simulations.

A. Generation rate due to sunlight absorption: $R_{E_{e(h)}}^{e(h),\text{sun}}$

Under the assumption of perfect absorption (where $w \gg$ absorption length), the number of photons absorbed into the absorber per unit time through surface area $\mathcal{A}$ is given by

$$\mathcal{A} \times \int_{E_g}^{\infty} j^{\text{sun}}(E) dE. \quad (4)$$

The solar spectrum for the photon number current (per unit area, per unit time, and per unit energy), $j^{\text{sun}}(E)$, is simply approximated using blackbody radiation at $T_S = 6000$ K under the AM0 condition [27],

$$j^{\text{sun}}(E) = \mathcal{CR} \times \frac{c}{4}\left(\frac{R_S}{L_{ES}}\right)^2 \mathcal{D}_\gamma^0(E) \times f_{0,\beta_S}^B(E), \quad (5)$$

where c is the speed of light in a vacuum ($= 3 \times 10^8$ m/s), $\hbar$ is Planck's constant/2π ($= 1.0545718 \times 10^{-34}$ J s), R_S is the solar radius ($= 0.696 \times 10^6$ km), L_{ES} is an average distance from the Earth to the Sun ($= 1.496 \times 10^8$ km), $\mathcal{CR}$ is the concentration ratio not greater than $(L_{ES}/R_S)^2 (= 46\,200)$, $\mathcal{D}_\gamma^0(E) = 1/(3\pi^2)(\hbar c)^{-3} \times 3E^2$ is the photonic density of states in a vacuum, and $f_{0,\beta_S}^B(E) = [\exp(\beta_S E) - 1]^{-1}$ is the Bose-Einstein distribution function at energy E with an inverse temperature $\beta_S = 1/(k_B T_S)$ given by the Sun's surface temperature $T_S (= 6000$ K) and Boltzmann constant $k_B (= 8.6 \times 10^{-5}$ eV/K).
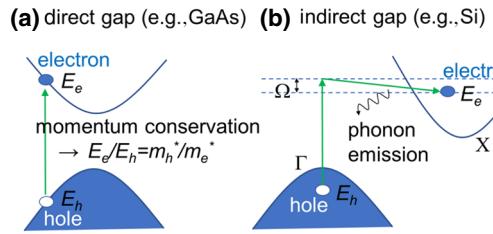

FIG. 4. Absorption processes in (a) direct and (b) indirect gap semiconductors.

If necessary, for practical device simulations, the solar spectrum may be replaced appropriately, e.g., using the AM1.5 spectrum normalized at a total power of 1 kWm^{-2}, which is not the case here [the 6000-K blackbody spectrum in Eqs. (4) and (5) approximates the AM0 spectrum at a total power of 1.6 kW/m^2 at 1 sun, with $\mathcal{CR} = 1$]. In the rate equations in Eqs. (1) and (2), the generation rates of the microscopic carrier distribution function $R_{E_{e(h)}}^{e(h),\text{sun}}$ should be expressed using the solar spectrum, $j^{\text{sun}}(E)$. The expression is dependent on whether the absorber is made from direct or indirect gap semiconductors (Fig. 4).

For direct gap semiconductor absorbers [Fig. 4(a)]—by considering momentum and energy conservations, we can equate the number of carriers that are generated in energy ranges of $E_e < E' < E_e + dE_e$ for electrons and $E_h < E' < E_h + dE_h$ for holes with the number of photons absorbed in the energy range $E < E' < E + dE$ per unit time in the absorber as follows:

$$\mathcal{A}j^{\text{sun}}(E)dE = \mathcal{D}_e(E_e)\mathcal{V}R_{E_e}^{e,\text{sun}}dE_e$$
$$= \mathcal{D}_h(E_h)\mathcal{V}R_{E_h}^{h,\text{sun}}dE_h, \quad (6)$$

where the energy conservation law gives $E = E_g + E_e + E_h$, and momentum conservation under the effective-mass approximation gives $E_e = (m_h^*/m_e^*)E_h$. $\mathcal{D}_e(= d_e\sqrt{E_e})$ and $\mathcal{D}_h(= d_h\sqrt{E_h})$ are the densities of states of electrons and holes per unit volume, where $d_{e(h)} = [2m_{e(h)}^*]^{3/2}/2\pi^2\hbar^3$ within a single band, isotropic effective-mass approximation under flatband conditions. The equation relates $R_{E_{e(h)}}^{e(h),\text{sun}}$ and $j^{\text{sun}}(E)$ directly, as follows:

$$R_{E_e}^{e,\text{sun}} = \frac{j^{\text{sun}}\left[E = E_g + (1 + m_e^*/m_h^*)E_e\right]}{w\mathcal{D}_e(E_e)}$$
$$\times \left(1 + \frac{m_e^*}{m_h^*}\right), \quad (7)$$

$$R_{E_h}^{h,\text{sun}} = \frac{j^{\text{sun}}\left[E = E_g + (1 + m_h^*/m_e^*)E_h\right]}{w\mathcal{D}_h(E_h)}$$
$$\times \left(1 + \frac{m_h^*}{m_e^*}\right), \quad (8)$$

where we assume that all microscopic states of carriers with the same energy are generated with equal probability, independent of their momentum directions. We, therefore, assume that the carrier distribution function is solely dependent on the kinetic energy of carriers and independent of the momentum direction. This assumption is used throughout the paper.

For indirect gap semiconductor absorbers [Fig. 4(b)]— the photon absorption process is accompanied by phonon emission or absorption. The energies of the electron-hole pairs deviate from the photon energy by the energy of one phonon [$(\Omega_{LA}, \Omega_{TA}, \Omega_{TO}) = (50.9, 57.4, 18.6)$ meV for Si]. We simply neglect the energy shift here because the phonon energy is much smaller than the spectral bandwidth, approximately $k_B T_S$, of the incoming sunlight. However, because the indirect transition accompanies a shift in the carrier momentum corresponding to the momentum carried by the phonons, momentum conservation among the photon and electron-hole pairs is not required in the absorption process. As a result, electron-hole pairs with arbitrary combinations of the energies E_e and E_h can be created by absorption of one photon with energy E, as long as $E = E_g + E_e + E_h$ is satisfied (where the phonon energy shift is neglected). The situation in indirect gap semiconductors means that the expressions for $R_{E_{e(h)}}^{e(h),\mathrm{sun}}$ from Eqs. (7) and (8) for direct gap semiconductors must be altered. Assuming that all electron-hole pairs with $E_e(< E - E_g)$ and $E_h(= E - E_g - E_e)$ are created by absorption of one photon with energy E with equal probability, the probability $p_{E_e}^e(E)dE_e$ of finding electrons in a small energy window $E_e < E' < E_e + dE_e$ immediately after absorption is

$$p_{E_e}^e(E)dE_e = \frac{\mathcal{D}_e(E_e)\mathcal{D}_h(\Delta E - E_e)dE_e}{\int_0^{\Delta E} \mathcal{D}_e(E')\mathcal{D}_h(\Delta E - E')dE'}, \quad (9)$$

where $\Delta E \equiv E - E_g$. Because the number of photons absorbed in the absorber per unit time and per unit energy is $\mathcal{A}j^{\mathrm{sun}}(E)$ for $E > E_g$, we find the following expression for the generation rate of electrons per microscopic state for indirect gap semiconductor absorbers:

$$\begin{aligned} R_{E_e}^{e,\mathrm{sun}} &= \frac{\int_{E_g}^\infty \mathcal{A}j^{\mathrm{sun}}(E) \times p_{E_e}^e(E)dE_e dE}{\mathcal{V}\mathcal{D}_e(E_e)dE_e} \\ &= \int_{E_g+E_e}^\infty \frac{j^{\mathrm{sun}}(E) \times \mathcal{D}_h(\Delta E - E_e)/w}{\int_0^{\Delta E} \mathcal{D}_e(E')\mathcal{D}_h(\Delta E - E')dE'}dE \\ &= \int_0^\infty \frac{j^{\mathrm{sun}}(E_g + E_e + E_h) \times \sqrt{E_h}}{\pi w d_e(E_e + E_h)^2/8}dE_h. \quad (10) \end{aligned}$$

The hole generation rate is given in a similar manner as

$$R_{E_h}^{h,\mathrm{sun}} = \int_0^\infty \frac{j^{\mathrm{sun}}(E_g + E_e + E_h) \times \sqrt{E_e}}{\pi w d_h(E_e + E_h)^2/8}dE_e. \quad (11)$$

B. Recombination loss rate: $R_{E_{e(h)}}^{e(h),\mathrm{rad}}$

The derivation of the expression for $R_{E_{e(h)}}^{e(h),\mathrm{rad}}$ presented in this subsection largely follows the derivations in the literature [27,28]. Because the absorber thickness w considered here is much smaller than the minority carrier diffusion length, we can safely assume a homogeneous carrier distribution inside the absorber. For a given set of carrier distribution functions, $\{n_{E_e}^e, n_{E_h}^h\}$, the recombination radiation rate, $r^{\mathrm{sp}}(E)$, of photons at photon energy E from the arbitrary position of a small volume inside the absorber into the whole solid angle (4π), per unit volume, per unit energy, and per unit time, is

$$\begin{aligned} r^{\mathrm{sp}}(E) &= \left(\frac{c}{n}\right)|\mathcal{M}|^2\mathcal{D}_\gamma^{\mathrm{cell}}(E)\int_0^{\Delta E}\mathcal{D}_e(E')\mathcal{D}_h(\Delta E - E') \\ &\quad \times n_{E'}^e n_{\Delta E - E'}^h dE', \quad (12) \end{aligned}$$

for the case of relaxed momentum selection rule (e.g., for an indirect gap semiconductor absorber and amorphous materials or nanostructures). Here, $\Delta E \equiv E - E_g$, c/n is the speed of light inside the absorber with refractive index n, $\mathcal{M}$ is proportional to the phonon-mediated transition matrix element that is approximated using the value at the absorption edge, and $\mathcal{D}_\gamma^{\mathrm{cell}}(E) = (1/3\pi^2)(\hbar c/n)^{-3} \times 3E^2$ is the photonic density of states in the absorber [29]. It is important to note that only part of the radiation, i.e., the radiation into the limited solid angle within the critical angle of total reflection ($\theta < \theta_c$), can escape from the absorber, as shown in Fig. 5, and this results in the photovoltaic current loss. The radiation rate $r^{sp(\pm)}(E)$ into the escape cones in the $\pm x$ direction, per unit volume, per unit energy, and per unit time, is then

$$\begin{aligned} r^{sp(\pm)}(E) &= \langle|(\vec{c}/n)\cdot\vec{e}_{\pm x}|\rangle_{\theta<\theta_c} \times |\mathcal{M}|^2\mathcal{D}_\gamma^{\mathrm{cell}}(E) \\ &\quad \times \int_0^{\Delta E}\mathcal{D}_e(E')\mathcal{D}_h(\Delta E - E')n_{E'}^e n_{\Delta E - E'}^h dE', \end{aligned}$$
$$(13)$$

where $\langle|(\vec{c}/n)\cdot\vec{e}_{\pm x}|\rangle_{\theta<\theta_c}$ represents the velocity of light in the $\pm x$ directions when averaged inside the escape cones,

$$\begin{aligned} \langle|\vec{c}/n\cdot\vec{e}_{\pm x}|\rangle_{\theta<\theta_c} &= \frac{c}{n} \times \frac{\int_0^{2\pi}d\varphi\int_0^{\theta_c}\cos\theta(\sin\theta d\theta)}{4\pi} \\ &= \frac{c(\sin\theta_c)^2}{4n} = \frac{1}{4}\left(\frac{c}{n}\right)\frac{1}{n^2}. \quad (14) \end{aligned}$$

The geometric average yields an expression for the rates that is independent of n, i.e.,

$$\begin{aligned} r^{sp(\pm)}(E) &= \frac{c}{4}|\mathcal{M}|^2\mathcal{D}_\gamma^0(E)\int_0^{\Delta E}\mathcal{D}_e(E')\mathcal{D}_h(\Delta E - E') \\ &\quad \times n_{E'}^e n_{\Delta E - E'}^h dE'. \quad (15) \end{aligned}$$

Under the same approximation using the constant transition matrix element $\mathcal{M}$, the absorption coefficient $\alpha(E)$ is given microscopically by

$$\alpha(E) = |\mathcal{M}|^2 \int_0^{\Delta E} \mathcal{D}_e(E')\mathcal{D}_h(\Delta E - E')$$
$$\times (1 - n_{E'}^e - n_{\Delta E - E'}^h)dE'. \quad (16)$$

Using the homogeneous radiation rate and absorption coefficient, we consider continuity equations for the photon number current density inside the absorber. Let $n_E^{\gamma(\pm)}$ and $j_E^{(\pm)}$ be the photon number density (per unit volume and per unit energy) and the photon number current density (per unit area, per unit time, and per unit energy) with energy E propagating in the $\pm x$ directions. Then, the continuity equations under the steady-state condition are given by

$$\partial_t n_E^{\gamma(\pm)} = \mp \partial_x j_E^{(\pm)}(x) + r^{sp(\pm)}(E) - \alpha(E)j_E^{(\pm)}(x)$$
$$= 0, \quad (17)$$

for $0 < x < w$ (Fig. 5). The continuity equations under the appropriate boundary conditions,

$$j_E^{(+)}(x \leq 0) = j_E^{sun}, \quad (18)$$

$$j_E^{(-)}(x \geq w) = 0, \quad (19)$$

give a solution for the output photon number current density,

$$j_E^{(+)}(x) = j_E^{sun}e^{-\alpha(E)x} + \frac{r^{sp(+)}(E)}{\alpha(E)}[1 - e^{-\alpha(E)x}], \quad (20)$$

$$j_E^{(-)}(x) = \frac{r^{sp(-)}(E)}{\alpha(E)}[1 - e^{\alpha(E)(x-w)}]. \quad (21)$$

Under the assumption of perfect absorption $[\alpha(E)w \gg 1]$ and zero reflection at the front surface, we thus have

$$j_E^{(+)}(x = w) = r^{sp(+)}(E)/\alpha(E), \quad (22)$$

$$j_E^{(-)}(x = 0) = r^{sp(-)}(E)/\alpha(E). \quad (23)$$

From this analysis, we can see that the photon number current output from the absorber does not depend on w, with the absorber's width $w \gg 1/\alpha(E)$ allowing for perfect absorption (hence, the radiative loss of charge current does not as well). This simply reflects the fact that recombination radiation and absorption of the emitted photons are balanced inside the absorber after cycles of the photon-recycling processes.

With Eqs. (22) and (23), the number of photons radiated out from the absorber per unit time ($\equiv dN_\gamma^{Rad}/dt$) through
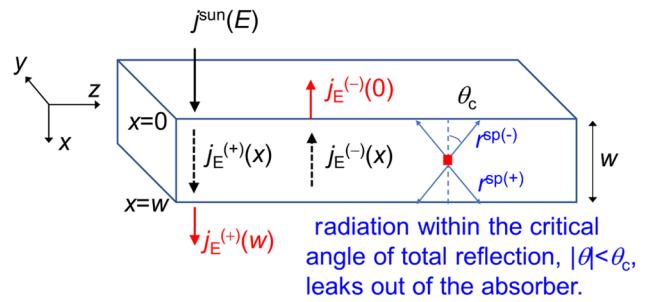
FIG. 5. Schematic for calculation of recombination loss rate, $R_{E_{e(h)}}^{e(h),rad}$.

the front and back surfaces is

$$\frac{dN_\gamma^{Rad}}{dt} = \mathcal{A}\int_{E_g}^{\infty}[j_E^{(+)}(x = w) + j_E^{(-)}(x = 0)]dE$$
$$= \frac{\mathcal{A}c}{2\pi^2}\left(\frac{1}{\hbar c}\right)^3 \int_{E_g}^{\infty} \frac{E^2\langle n^e n^h\rangle_{\Delta E}}{\langle 1 - n^e - n^h\rangle_{\Delta E}}dE, \quad (24)$$

where Eqs. (15) and (16) are inserted, and

$$\langle n^e n^h\rangle_{\Delta E}$$
$$\equiv \frac{\int_0^{\Delta E} \mathcal{D}_e(E')\mathcal{D}_h(\Delta E - E')n_{E'}^e n_{\Delta E - E'}^h dE'}{\int_0^{\Delta E} \mathcal{D}_e(E')\mathcal{D}_h(\Delta E - E')dE'}, \quad (25)$$

$$\langle 1 - n^e - n^h\rangle_{\Delta E}$$
$$\equiv \frac{\int_0^{\Delta E} \mathcal{D}_e(E')\mathcal{D}_h(\Delta E - E')(1 - n_{E'}^e - n_{\Delta E - E'}^h)dE'}{\int_0^{\Delta E} \mathcal{D}_e(E')\mathcal{D}_h(\Delta E - E')dE'}.$$
$$(26)$$

When the carriers are in thermal equilibrium so that the distribution function is given by the Fermi-Dirac distributions
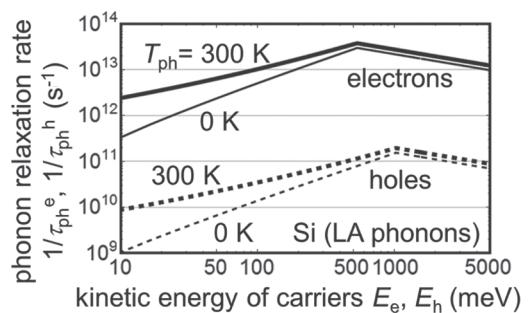
FIG. 6. Estimation of phonon relaxation rate of carriers via the LA mode in Si as estimated from Eq. (39) as a function of kinetic energy for the electrons (solid) and holes (dashed) at two different lattice temperatures: $T_{ph} = 300$ K (thick) and 0 K (thin). The following parameters are used for Si (found in a standard textbook [41]): $v_A = 10^4$ m/s, $m_e^*/m_e = 1.08$, $m_h^*/m_e = 0.55$, $\epsilon_{cut}^{ph} = 50$ meV, $a_{def,c} = 10$ eV, $a_{def,v} = 1$ eV, and $\rho_A = 2.3$ g/cm^3.

with inverse temperature β, and chemical potentials μ_c and $\mu_h (= -\mu_v)$, following relationship

$$\frac{1 - n^e_{E'} - n^h_{\Delta E - E'}}{n^e_{E'} n^h_{\Delta E - E'}} = e^{\beta[E - (\mu_c - \mu_v)]} - 1, \qquad (27)$$

is fulfilled for every possible choice of $E(\equiv \Delta E + E_g)$ and E' in Eq. (26). The integrand in Eq. (24) is then found to be

$$\frac{E^2 \langle n^e n^h \rangle_{\Delta E}}{\langle 1 - n^e - n^h \rangle_{\Delta E}} = \frac{E^2}{e^{\beta(E - (\mu_c - \mu_v))} - 1}. \qquad (28)$$

In this way, Eq. (24) safely reproduces the generalized Planck law under the thermal equilibrium, and we can understand that Eq. (24) is an extension to nonequilibrium regimes with nonequilibrium carrier distribution for the case of the relaxed momentum selection rule.

Given that the band-filling effect can be neglected with $n^{e(h)}_{E_{e(h)}} \ll 1$, Eq. (24) is approximated using

$$\frac{dN^{\text{Rad}}_\gamma}{dt} \approx \frac{\mathcal{A}c}{2\pi^2} \left(\frac{1}{\hbar c}\right)^3 \int_{E_g}^\infty E^2 \langle n^e n^h \rangle_{\Delta E} dE. \qquad (29)$$

Because the radiative loss of one photon is equal to the loss of one electron-hole pair, $dN^{\text{Rad}}_\gamma / dt$ can be related to $R^{e(h),\text{rad}}_{E_{e(h)}}$.

For indirect gap semiconductor absorbers—the above results for the case of the relaxed momentum selection rule can be used directly. Part of $dN^{\text{Rad}}_\gamma / dt$ in Eq. (28) with Eq. (25), which comes from recombination of the electrons (holes) in a small energy window, $E_{e(h)} < E' < E_{e(h)} + dE_{e(h)}$, divided by the number of corresponding electron (hole) states, $\mathcal{V} \mathcal{D}^{e(h)}_{E_{e(h)}} dE_{e(h)}$, gives the radiation loss rates for the microscopic carrier distribution functions. This produces the following expressions:

$$R^{e,\text{rad}}_{E_e} = \frac{c}{2\pi^2 w} \left(\frac{1}{\hbar c}\right)^3$$
$$\times \int_0^\infty \frac{(E_g + E_e + E_h)^2 \sqrt{E_h} \times n^e_{E_e} n^h_{E_h}}{(\pi/8) d_e (E_e + E_h)^2} dE_h, \quad (30)$$

$$R^{h,\text{rad}}_{E_h} = \frac{c}{2\pi^2 w} \left(\frac{1}{\hbar c}\right)^3$$
$$\times \int_0^\infty \frac{(E_g + E_e + E_h)^2 \sqrt{E_e} \times n^e_{E_e} n^h_{E_h}}{(\pi/8) d_h (E_e + E_h)^2} dE_e. \quad (31)$$

For direct gap semiconductor absorbers—taking the momentum conservation discussed in Sec. II A into account, the radiation loss rates for the microscopic carrier

distribution functions are obtained using a similar analysis. Here we simply show the final results:

$$R^{e,\text{rad}}_{E_e} = \frac{c}{2\pi^2 w} \left(\frac{1}{\hbar c}\right)^3 \frac{(E_g + E_e + E_h)^2}{d_e \sqrt{E_e}}$$
$$\times \left(1 + \frac{m^*_e}{m^*_h}\right) \frac{n^e_{E_e} n^h_{E_h}}{1 - n^e_{E_e} - n^h_{E_h}} \Bigg|_{E_h = \frac{m^*_e}{m^*_h} E_e}, \quad (32)$$

$$R^{h,\text{rad}}_{E_h} = \frac{c}{2\pi^2 w} \left(\frac{1}{\hbar c}\right)^3 \frac{(E_g + E_e + E_h)^2}{d_h \sqrt{E_h}}$$
$$\times \left(1 + \frac{m^*_h}{m^*_e}\right) \frac{n^e_{E_e} n^h_{E_h}}{1 - n^e_{E_e} - n^h_{E_h}} \Bigg|_{E_e = \frac{m^*_h}{m^*_e} E_h}. \quad (33)$$

Insertion of $1 - n^e_{E_e} - n^h_{E_h} \approx 1$ into the denominators in Eqs. (32) and (33) gives approximate expressions for direct gap semiconductors that correspond to Eqs. (30) and (31) for indirect gap semiconductors.

C. Carrier extraction rate: $R^{e(h),\text{out}}_{E_{e(h)}}$

Carrier extraction from an absorber to an electrode is a result of the carrier transfer between them, which can be treated in our model as the interaction between carrier system and electron or hole reservoirs (bath 1 or 2) in Fig. 1. As derived in Appendix A, we obtain the net extraction rate $R^{e(h),\text{out}}_{E_{e(h)}}$ in Eqs. (1) and (2) in a weak interaction case. In the derivation, we assume that carriers in the electrodes are in the thermal equilibrium, where we can define the temperature T_c and the Fermi levels, μ_c and $-\mu_v$. This means that their distribution functions are given by the Fermi-Dirac distribution functions with these parameters, $f^F_{\mu_c, \beta_c}$ and $f^F_{-\mu_v, \beta_c}$. As explained in Appendix A, within the second-order perturbation theory with respect to the system-bath interaction, we find the results of Fermi's golden rule for the net extraction rate,

$$R^{e,\text{out}}_{E_e} = \frac{1}{\tau^e_{\text{out}}} \left[n^e_{E_e} - f^F_{\mu_c, \beta_c}(E_g + E_e)\right], \qquad (34)$$

$$R^{h,\text{out}}_{E_h} = \frac{1}{\tau^h_{\text{out}}} \left[n^h_{E_h} - f^F_{-\mu_v, \beta_c}(E_h)\right], \qquad (35)$$

with extraction times τ^e_{out} and τ^h_{out} that are defined as

$$(\tau^e_{\text{out}})^{-1} = \frac{2\pi}{\hbar} |T^e(E)|^2 \mathcal{D}_c(E) \Bigg|_{E = E_g + E_e}, \qquad (36)$$

$$(\tau^h_{\text{out}})^{-1} = \frac{2\pi}{\hbar} |T^h(E)|^2 \mathcal{D}_d(E) \Bigg|_{E = E_h}. \qquad (37)$$

Here, $\mathcal{D}_c(E)[= \sum_{k'} \delta(E - \epsilon^c_{k'})]$ and $\mathcal{D}_d(E)[= \sum_{k'} \delta(E - \epsilon^d_{k'})]$ are the density of states in electron and hole reservoirs in Fig. 1, and $|T^e(E)|^2$ and $|T^h(E)|^2$ are the effective

tunneling probability for electrons and holes. In the following, we also assume the simplest case, i.e., where $\tau_{\text{out}}^{e} = \tau_{\text{out}}^{h} \equiv \tau_{\text{out}}$, which will not limit the generality of the main conclusion.

According to its derivation, τ_{out} should be regarded as the effective time scale used for carrier extraction, which is defined at the contact by the tunneling rate. However, in the rate Eqs. (1) and (2), the extraction terms in Eqs. (34) and (35) relax the distribution functions to those in the electrodes within the time τ_{out}. Therefore, it could also be used to parametrize the time between photogeneration and extraction of the carriers, which should present in real devices for some other reasons; e.g., when photogeneration occurs at the center of the absorber, τ_{out} cannot be less than the time delay given by the distance from the point of generation to the contacts divided by the average carrier velocity. Such time delays would be important in thicker solar cells and appear to be critical in solar cells using nanocrystals, organic solar cells [30,31] (including dye-sensitized [32]), and perovskite solar cells [33], which have low carrier mobilities caused by disorders and the Frenkel-like localization [34,35] of excitons. τ_{out} could be measured using specific characterization methods that are suitable for each system, e.g., by optical characterization of the lifetimes of photogenerated carriers under short-circuit conditions and by transient measurement of the photocurrents [36,37].

Having considered above, from here in this paper, we shall regard τ_{out} as a phenomenological parameter, which represents the time scale the carriers spend until they are extracted in the contacts after the generation (i.e., dwell time spent in the absorber), though it is derived differently based on the tunnel Hamiltonian [Eq. (A15) in Appendix A]. This point will be discussed again in Sec. III C. While the time spent in the absorber can be introduced in this way, the present theory cannot tell the impact of the inhomogeneous carrier distribution, strong built-in fields, and nonlocal correlation in the charge transport, which can affect solar-cell properties in the presence of low-mobility materials and nanostructures [38–40]. Therefore, we focus only on the former effect, and realistic modeling will be required to include the latter effects (e.g., by nonequilibrium Green functions). Regardless of the simplified time-scale argument, our approach allows the depiction of various effects that can alter the device characteristics and the nonequilibrium energy distribution functions, giving a comprehensive understanding on the device physics in terms of this time scale, as will become clear by the simulations shown later.

D. Phonon scattering (thermalization) rate: $R_{E_{e(h)}}^{e(h),\text{phonon}}$

Phonon scattering rate $R_{E_{e(h)}}^{e(h),\text{phonon}}$ in the rate equations can be derived in a similar manner as explained

in Appendix A for the extraction rate $R_{E_{e(h)}}^{e(h),\text{out}}$, i.e., by taking into account the system-bath coupling within the second-order perturbation theory, i.e., by Fermi's golden rule approach. In this case, the system and bath correspond, respectively, to carriers and phonons in the absorber, i.e., carrier system and phonon reservoir (bath 3) in Fig. 1. Its microscopic derivation is given in detail in Appendix B. Here we just show the final result in the energy representation,

$$R_{E_{e(h)}}^{e(h),\text{phonon}}$$

$$
\begin{aligned}
= &\int_{0}^{\epsilon_{\text{cut}}^{e(h),-}} W_{E_{e(h)},E_{e(h)}-\epsilon}^{-} \{ n_{E_{e(h)}}^{e(h)} \left[1 - n_{E_{e(h)}-\epsilon}^{e(h)} \right] \\
&\times \left[1 + f_{0,\beta_{\text{ph}}}^{B}(\epsilon) \right] - n_{E_{e(h)}-\epsilon}^{e(h)} [1 - n_{E_{e(h)}}^{e(h)}] f_{0,\beta_{\text{ph}}}^{B}(\epsilon) \} d\epsilon \\
&- \int_{0}^{\epsilon_{\text{cut}}^{e(h),+}} W_{E_{e(h)}+\epsilon,E_{e(h)}}^{+} \{ n_{E_{e(h)}+\epsilon}^{e(h)} [1 - n_{E_{e(h)}}^{e(h)}] \\
&\times [1 + f_{0,\beta_{\text{ph}}}^{B}(\epsilon)] - n_{E_{e(h)}}^{e(h)} [1 - n_{E_{e(h)}+\epsilon}^{e(h)}] f_{0,\beta_{\text{ph}}}^{B}(\epsilon) \} d\epsilon.
\end{aligned}
\tag{38}
$$

For LA phonon scattering considered in this paper, the transition rates per unit energy are given by

$$W_{E_{e(h)},E_{e(h)}-\epsilon}^{-} = C_{\text{ph}}^{e(h)} \frac{\epsilon^2}{\sqrt{E_{e(h)}}}, \tag{39}$$

$$W_{E_{e(h)}+\epsilon,E_{e(h)}}^{+} = C_{\text{ph}}^{e(h)} \frac{\epsilon^2}{\sqrt{E_{e(h)}}}, \tag{40}$$

with a coefficient $C_{\text{ph}}^{e(h)} \equiv a_{\text{def},c(v)}^{2} \sqrt{m_{e(h)}^{*}/2} 4\pi \hbar^4 v_A^4 \rho_A$, where $a_{\text{def},c(v)}$, v_A, and ρ_A are the deformation potential for the conduction (valence) electrons, the phonon velocity, and the mass density in the absorber, respectively. High-energy cutoffs $\epsilon_{\text{cut}}^{e(h),\pm}$ in the integration range in Eq. (38), i.e., Eqs. (B9) and (B10) in Appendix B, depend on the Debye cutoff, effective mass and energy of carriers, and phonon velocity. This originates from the momentum and energy conservation at the phonon scattering event.

The time scale for thermalization of the photogenerated carriers in the absorber can be estimated from Eq. (B8). Consider the case where electrons (holes) with energy $E_{e(h)}$ are generated at an initial time $t = 0$ under illumination by a narrow-band photon source at the corresponding energy. In this case, $n_{E_{e(h)}}^{e(h)} \neq 0$ and $n_{E \neq E_{e(h)}}^{e(h)} = 0$ at $t = 0$. When this condition is inserted into Eq. (B8), the initial population dynamics are given by

$$\frac{d}{dt} n_{E_{e(h)}}^{e(h)} = -\frac{1}{\tau_{\text{ph}}^{e(h)}} n_{E_{e(h)}}^{e(h)}, \tag{41}$$

where the relaxation time $\tau_{\rm ph}^{e(h)}$ is given by

$$\frac{1}{\tau_{\rm ph}^{e(h)}} = C_{\rm ph}^{e(h)} \left\{ \int_0^{\epsilon_{\rm cut}^{e(h),-}} \frac{\epsilon^2 [1 + f_{0,\beta_{\rm ph}}^B(\epsilon)]}{\sqrt{E_{e(h)}}} d\epsilon \right.$$
$$\left. + \int_0^{\epsilon_{\rm cut}^{e(h),+}} \frac{\epsilon^2 f_{0,\beta_{\rm ph}}^B(\epsilon)}{\sqrt{E_{e(h)}}} d\epsilon \right\}. \qquad (42)$$

At the zero temperature of the lattice, insertion of $f_{0,\beta_{\rm ph}=+\infty}^B(\epsilon) = 0$ into Eq. (42) gives the simple expression

$$\frac{1}{\tau_{\rm ph}^{e(h)}} = C_{\rm ph}^{e(h)} \frac{[\epsilon_{\rm cut}^{e(h),-}]^3}{3\sqrt{E_e(h)}}. \qquad (43)$$

Of course, the time constant $\tau_{\rm ph}^{e(h)}$ gives a time scale for the initial relaxation dynamics for such an ideal situation. It, therefore, seems reasonable to consider that the carrier thermalization time in solar cells could also be estimated using $\tau_{\rm ph}^{e(h)}$ in Eq. (42). Fig. 6 shows the phonon relaxation rate that is estimated for Si as a function of the kinetic energies of the carriers. In our Si model, we find that the relaxation time ranges between 10^{-10} and $10^{-13.5}$ s in the relevant energy window for solar cells (as shown in Fig. 5 that corresponds to the bandwidth of the solar spectra, $k_B T_S$). This result is consistent with the measured time scale for the carrier cooling process, which ranges from subpicosecond to hundreds of picoseconds [42–44] and also with the time scales in the literature [45]. A major difference (two orders of magnitude) between the results for electrons and holes originates from differences in the deformation potentials for the LA phonons. The situation can, therefore, change if other phonon modes and the fast electron-hole equilibration that was discussed in [42] are taken into account in the calculations. From this perspective, we should stress here that the results in Fig. 6 are given for an order of magnitude-level estimation (as mentioned also in Appendix B).

E. Effects of spectral broadening of the microscopic states

In the previous four subsections (Secs. II A, II B, II C, II D), explicit forms of the rate equation for the microscopic carrier distribution function in both Eqs. (1) and (2) appear to be found. Actually, as shown in the simulations below, direct use of the equations that have been derived thus far can be justified in most cases. However, in some cases, the equations should be modified slightly. Modifications are required when the spectral broadening of the microscopic carrier states becomes important, as it occurs naturally due to carrier extraction and relaxation and can modify the recombination emission property and current-voltage characteristics of the device. These

situations occur when the carriers are far out of equilibrium (in fast extraction regime III in Sec. III C; see the simulations in Sec. IV). The spectral broadening Γ is taken into account in the NEGF formalism automatically as an imaginary part of the (retarded) self-energy ($\Gamma = -\text{Im}\Sigma^r$) [9–11]. Therefore, we also take the broadening effect into account in a satisfactory manner while keeping the calculations as simple as possible.

Several factors can broaden the spectra of the single-particle states in many-particle systems. One factor comes from Coulomb interaction between the carriers. However, we consider the Coulomb interaction to have a minor or secondary effect on the properties of solar cells, which normally work at low carrier densities (as shown for Si solar cells in [2]), and we have already neglected to include it in our model. Other factors occur because of interactions between the carrier system and the baths, or more explicitly, because of the carrier-phonon interaction and carrier extraction processes that occur in our model. Spectral broadening of the electrons (holes) with $E_{e(h)}$, given by $\Gamma_{E_{e(h)}}^{e(h)}\{\equiv -\text{Im}\Sigma^r[E_{e(h)}]\}$, is related to the time constants $\tau_{\rm out}^{e(h)}(= \tau_{\rm out})$ and $\tau_{\rm ph}^{e(h)}$, which we already determined in the preceding subsections:

$$\Gamma_{E_{e(h)}}^{e(h)} = \frac{\hbar}{2\tau_{\rm ph}^{e(h)}} + \frac{\hbar}{2\tau_{\rm out}^{e(h)}}. \qquad (44)$$

Therefore, the broadening is given by $\hbar/[2\tau_{\rm ph}^{e(h)}]$ when $\tau_{\rm ph}^{e(h)} \ll \tau_{\rm out}^{e(h)}$ and $\hbar/[2\tau_{\rm out}^{e(h)}]$ when $\tau_{\rm out}^{e(h)} \ll \tau_{\rm ph}^{e(h)}$.

In the former case [$\tau_{\rm ph}^{e(h)} \ll \tau_{\rm out}^{e(h)}$], it is natural to consider that the carriers must be fully relaxed to establish thermal equilibrium with the lattice in the steady state. This assumption can be checked by solving the rate equations in Eqs. (1) and (2) as follows. When the thermalization term $R_{E_{e(h)}}^{e(h),\text{phonon}}$ dominates the rate equation, a steady state is achieved when all integrands in Eq. (B8) disappear. This condition is fulfilled if

$$\left[\frac{n_{E_{e(h)}+\epsilon}^{e(h)}}{1 - n_{E_{e(h)}+\epsilon}^{e(h)}} \right] / \left[\frac{n_{E_{e(h)}}^{e(h)}}{1 - n_{E_{e(h)}}^{e(h)}} \right]$$
$$= \frac{f_{0,\beta_{\rm ph}}^B(\epsilon)}{1 + f_{0,\beta_{\rm ph}}^B(\epsilon)} = \exp\{-\beta_{\rm ph}\epsilon)$$
$$= \exp(-\beta_{\rm ph}[E_{e(h)} + \epsilon]\}/\exp[-\beta_{\rm ph}E_{e(h)}] \qquad (45)$$

for every possible choice of $E_{e(h)}$ and ϵ. This means that in the steady state, the distribution function is given by the Fermi-Dirac distribution, with some value for the chemical potential in the absorber $\mu_{e(h)}^{\rm cell}$:

$$n_{E_{e(h)}}^{e(h)} = f_{\mu_{e(h)}^{\rm cell},\beta_{\rm ph}}^F[E_{e(h)}]. \qquad (46)$$

Therefore, these distribution functions are thermally distributed over the energy range $0 < E_{e(h)} < k_B T_{\rm ph}$. In this case, inclusion of the broadening within the single-particle spectra does not modify the distribution function as long as $\Gamma_{E_{e(h)}}^{e(h)} \left\{ = \hbar/[2\tau_{\rm ph}^{e(h)}] \right\} < k_B T_{\rm ph} (= 26 \text{ meV for } 300/\text{K})$. The condition appears to be satisfied well when we consider that a phonon relaxation time of 1 ps corresponds to broadening of 0.33 meV. In this way, we confirm that the broadening effect is negligible for $\tau_{\rm ph}^{e(h)} \ll \tau_{\rm out}^{e(h)}$.

The above consideration allows us to neglect broadening due to electron-phonon interactions in Eq. (44) over the entire range of $\tau_{\rm out}^{e(h)}$. We can therefore safely use the following approximation:

$$\Gamma_{E_{e(h)}}^{e(h)} = \frac{\hbar}{2\tau_{\rm out}^{e(h)}}. \tag{47}$$

This approximation greatly simplifies the calculations because $\tau_{\rm out}^{e(h)} (= \tau_{\rm out})$ is a given parameter that is identical for every carrier state in our model, whereas $\tau_{\rm ph}^{e(h)}$, which should be defined precisely from Eq. (B8), is a function of the carrier distribution functions that are to be determined finally. We therefore use an approximation based on use of Eq. (47) for broadening of the single-particle states in this work. We define the lineshape function of the states using $\mathcal{A}_\Gamma(x)$, which is a Gaussian function with a half width at half maximum that is equal to $\Gamma_{E_{e(h)}}^{e(h)}$. Using $\Gamma \equiv (\log 2)^{-1/2} \Gamma_{E_{e(h)}}^{e(h)}$, the function is given by

$$\mathcal{A}_\Gamma(x) = \sqrt{\frac{1}{\pi \Gamma^2}} \exp[-(x/\Gamma)^2]. \tag{48}$$

A Lorentzian function is normally used for the lineshape of a single-particle state (this also applies in the NEGF formalism [13]) rather than a Gaussian spectral profile because the Gaussian distribution reflects the statistical fluctuations of the system; it is not derived naturally for ideal models without structural imperfections. We use the Gaussian function for a reason that is demonstrated in Appendix C; however, it will not change our main conclusion.

F. Macroscopic properties: current, conversion efficiency, and energy flow

The rate equations used to determine the microscopic carrier distribution functions are derived in the preceding subsections (from Sec. II A to Sec. II E). In this section, we briefly summarize the method used to calculate macroscopic quantities such as the output charge current I, the conversion efficiency η, and the energy flows into the different channels, denoted by P_X ($X = $ sun, T, rad, work, $Q_{\rm in}$, and $Q_{\rm out}$ are defined below and are also shown in
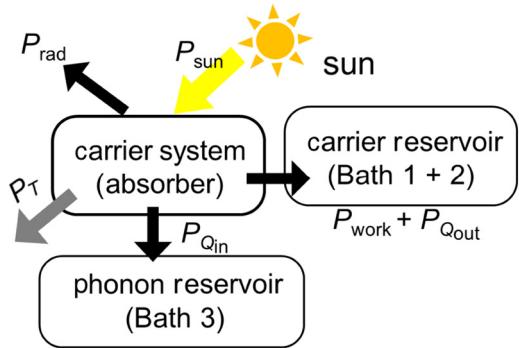

FIG. 7. Energy current from the Sun $P_{\rm sun}$, which is shared by five energy current channels: radiation $P_{\rm rad}$, light transmission P_T, output work $P_{\rm work}$, heat passing into the electrodes $P_{Q_{\rm out}}$, and heat passing into the absorber crystal lattice $P_{Q_{\rm in}}$.

Fig. 7) in terms of the distribution functions that are to be obtained.

The charge current I is defined as

$$I = |e| \sum_k R_{E_e(k)}^{e,{\rm out}} = |e| \sum_k R_{E_h(k)}^{h,{\rm out}}$$

$$= |e| \int_0^\infty \mathcal{V} \mathcal{D}_e(E_e) R_{E_e}^{e,{\rm out}} dE_e, \tag{49}$$

which represents the total charge per unit time (where $|e|$ is the elementary charge) output by an absorber of volume $\mathcal{V}(= \mathcal{A}w)$ to an electrode. Here $R_{E_e}^{e,{\rm out}}$ and $R_{E_h}^{h,{\rm out}}$ are the functions of the distribution functions given by Eqs. (A24) and (A27) without the broadening effect, and of the functions given by Eqs. (C13) and (C14) with the broadening effect, respectively. The second equation in Eq. (49) comes from the steady-state condition based on the total number of charges in the absorber (and will be mentioned again as Eqs. (76) in Sec. III). Given that the conduction electrons are extracted to the electrode with chemical potential μ_c and the valence holes are extracted to the electrode with potential μ_v ($-\mu_v$ for holes), the total output energy per unit time is given by

$$\mathcal{P}_{\rm work} = (\mu_c - \mu_v)I = VI, \tag{50}$$

which defines the conversion efficiency as

$$\eta(\%) = \frac{\mathcal{P}_{\rm work}}{\mathcal{A} \times \int_0^\infty E j^{\rm sun}(E) dE} \times 100. \tag{51}$$

This expression indicates that the conversion efficiency is dependent on the absorber thickness w because I and $\mathcal{P}_{\rm work}$ are both proportional to $\mathcal{V}$ from Eq. (49).

The microscopic carrier distribution function offers more detailed information about the energy balance of the solar cells. This information is very helpful in understanding what occurs inside solar cells during the energy

conversion processes, which could also be addressed experimentally [46]. The energy current P_X (per unit time per unit area) that flows into each channel X can be evaluated separately using the steady-state solution as follows (see also Fig. 7). They are defined by considering the total energy current that leaks out from the absorber's carrier system,

$$
\begin{aligned}
\frac{d}{dt}\langle H_{0,\mathrm{sys}}\rangle &= \sum_k [E_g + E_e(k)]\frac{d}{dt}\langle e_k^\dagger e_k\rangle \\
&\quad + \sum_k E_h(k)\frac{d}{dt}\langle h_k^\dagger h_k\rangle \\
&= \sum_k [E_g + E_e(k)]\frac{d}{dt}n_k^e + \sum_k E_h(k)\frac{d}{dt}n_k^h \\
&= \mathcal{V}\int \mathcal{D}_e(E_e)(E_g + E_e)\frac{d}{dt}n_{E_e}^e dE_e \\
&\quad + \mathcal{V}\int \mathcal{D}_h(E_h)E_h\frac{d}{dt}n_{E_h}^h dE_h \\
&= \mathcal{V}\int \mathcal{D}_e(E_e)(E_g + E_e)(R_{E_e}^{e,\mathrm{sun}} - R_{E_e}^{e,\mathrm{rad}} \\
&\quad - R^{e,\mathrm{out}} - R_{E_e}^{e,\mathrm{phonon}})dE_e + \mathcal{V}\int \mathcal{D}_h(E_h)E_h \\
&\quad \times \left(R_{E_h}^{h,\mathrm{sun}} - R_{E_h}^{h,\mathrm{rad}} - R_{E_h}^{h,\mathrm{out}} - R_{E_h}^{h,\mathrm{phonon}}\right)dE_h \\
&\equiv \mathcal{A}\left[(P_{\mathrm{sun}} - P_T) - P_{\mathrm{rad}} - P_{\mathrm{out}} - P_{Q_{\mathrm{in}}}\right] \\
&= 0,
\end{aligned}
\tag{52}
$$

where the energy current per unit time per unit area into each channels are thus defined by

$$
\begin{aligned}
P_{\mathrm{sun}} - P_T &\equiv w\int \mathcal{D}_e(E_e)(E_g + E_e)R_{E_e}^{e,\mathrm{sun}}dE_e \\
&\quad + w\int \mathcal{D}_h(E_h)E_h R_{E_h}^{h,\mathrm{sun}}dE_h,
\end{aligned}
\tag{53}
$$

$$
\begin{aligned}
P_{\mathrm{rad}} &\equiv w\int \mathcal{D}_e(E_e)(E_g + E_e)R_{E_e}^{e,\mathrm{rad}}dE_e \\
&\quad + w\int \mathcal{D}_h(E_h)E_h R_{E_h}^{h,\mathrm{rad}}dE_h,
\end{aligned}
\tag{54}
$$

$$
\begin{aligned}
P_{\mathrm{out}} &\equiv w\int \mathcal{D}_e(E_e)(E_g + E_e)R_{E_e}^{e,\mathrm{out}}dE_e \\
&\quad + w\int \mathcal{D}_h(E_h)E_h R_{E_h}^{h,\mathrm{out}}dE_h,
\end{aligned}
\tag{55}
$$

$$
\begin{aligned}
P_{Q_{\mathrm{in}}} &\equiv w\int \mathcal{D}_e(E_e)(E_g + E_e)R_{E_e}^{e,\mathrm{phonon}}dE_e \\
&\quad + w\int \mathcal{D}_h(E_h)E_h R_{E_h}^{h,\mathrm{phonon}}dE_h.
\end{aligned}
\tag{56}
$$

They can be further evaluated by inserting the rates $R_{E_{e(h)}}^{e(h),X}$ (obtained in the preceding subsections) and performing the integration.

The last equation in Eq. (52) means that the energy current that is carried by the photons that illuminate the solar cell

$$
P_{\mathrm{sun}} = \int_0^\infty Ej^{\,\mathrm{sun}}(E)dE,
\tag{57}
$$

is shared by different flow channels (five channels are present in this model):

$$
P_{\mathrm{sun}} = P_{\mathrm{T}} + P_{\mathrm{rad}} + P_{\mathrm{work}} + P_{Q_{\mathrm{out}}} + P_{Q_{\mathrm{in}}},
\tag{58}
$$

where we further decomposed P_{out} in Eq. (52) into work and heat by $P_{\mathrm{out}} = P_{\mathrm{work}} + P_{Q_{\mathrm{out}}}$.

The proportion of the solar energy, P_T, per unit time per unit area, that is transmitted is given by

$$
P_T = \int_0^{E_g} Ej^{\,\mathrm{sun}}(E)dE.
\tag{59}
$$

Here, the absorption spectrum of the absorber is approximated simply using the step function $\alpha(E) = \alpha_0\theta(E - E_g)$ under the assumption of perfect absorption $\alpha_0 w \gg 1$ (or a large effective light path $l_{\mathrm{eff}} \gg 1/\alpha_0$ with light trapping textures [47]).

The energy that is radiated outside the solar cell per unit time per unit area is then given by

$$
P_{\mathrm{rad}} = \frac{c}{2\pi^2}\left(\frac{1}{\hbar c}\right)^3 \int_0^\infty E^2\langle En^e n^h\rangle_{\Delta E}dE,
\tag{60}
$$

where $\Delta E \equiv E - E_g$, and $1 - n_{E_e}^e - n_{E_h}^h \approx 1$ is used. When the broadening effect is taken into account, $\langle En^e n^h\rangle_{\Delta E}$ in the integrand is given by

$$
\begin{aligned}
\langle En^e n^h\rangle_{\Delta E} &= \int_0^\infty \int_0^\infty p_{E_e,E_h}^{\Delta E}(E_g + E_{eh}) \\
&\quad \times n_{E_e}^e n_{E_h}^h dE_e dE_h,
\end{aligned}
\tag{61}
$$

where $E_{eh} \equiv E_e + E_h$ and $p_{E_e,E_h}^{\Delta E}$ is a weight function that is defined by

$$
p_{E_e,E_h}^{\Delta E} \equiv \frac{\mathcal{D}_e(E_e)\mathcal{D}_h(E_h)\mathcal{A}_{\sqrt{2}\Gamma}(\Delta E - E_e - E_h)}{\iint \mathcal{D}_e(E_e)\mathcal{D}_h(E_h)\mathcal{A}_{\sqrt{2}\Gamma}(\Delta E - E_e - E_h)dE_e dE_h}
\tag{62}
$$

for indirect gap semiconductors. For the direct gap semiconductors, $\langle En^e n^h\rangle_{\Delta E}$ is given by

$$
\langle En^e n^h\rangle_{\Delta E} = \int_0^\infty p_{E_{eh}}^{\Delta E}(E_g + E_{eh})n_{E_e}^e n_{E_h}^h dE_{eh},
\tag{63}
$$

with a weight function that is defined by

$$p_{E_{eh}}^{\Delta E} \equiv \frac{\sqrt{E_{eh}}\mathcal{A}_{\sqrt{2}\Gamma}(\Delta E - E_{eh})}{\int_0^\infty \sqrt{E'_{eh}}\mathcal{A}_{\sqrt{2}\Gamma}(\Delta E - E'_{eh})dE'_{eh}}, \qquad (64)$$

where $\Delta E \equiv E - E_g$, $m_e^* E_e = m_h^* E_h$. In a similar manner to the discussion in Appendix C, the expressions above can be used in the limit where $\Gamma = +0$ by changing the lineshape functions in the integrand into delta functions.

P_{work} is the energy that is extracted as work from the solar cell (per unit time per unit area) and transferred via the charge current, which we already evaluated earlier, and is given by

$$P_{\text{work}} = \mathcal{P}_{\text{work}}/\mathcal{A}$$
$$= w|e|V \int_0^\infty \mathcal{D}_e(E_e) R_{E_e}^{e,\text{out}} dE_e. \qquad (65)$$

$P_{Q_{\text{out}}}$ is the heat that is carried by the charge current and lost in the electrodes outside the cell per unit time per unit area. It can be calculated as

$$P_{Q_{\text{out}}} \equiv P_{\text{out}} - P_{\text{work}}$$
$$= \frac{w}{\tau_{\text{out}}} \iint \mathcal{D}^e(E_e) \times (E_g + E_e - \mu_c)$$
$$\times \mathcal{A}_\Gamma(\Delta E - E_e) \times \left[n_{E_e}^e - f_{\mu_c,\beta_c}^F(E)\right] dE_e dE$$
$$+ \frac{w}{\tau_{\text{out}}} \iint \mathcal{D}^h(E_h) \times [E_h - (-\mu_v)] \times \mathcal{A}_\Gamma(E - E_h)$$
$$\times \left[n_{E_h}^h - f_{-\mu_v,\beta_c}^F(E)\right] dE_h dE, \qquad (66)$$

where $\Delta E \equiv E - E_g$, and the integration runs over the ranges $-\infty < E < \infty$ and $0 < E_{e(h)} < \infty$.

The remaining channel for the energy loss in our model is the absorber thermalization loss that is lost in the phonon reservoir (bath 3 in Fig. 1). $P_{Q_{\text{in}}}$ is this heat current, which is lost in the phonon bath, inside the cell per unit time per unit area. It is convenient to determine $P_{Q_{\text{in}}}$ using the energy conservation law given in Eq. (58),

$$P_{Q_{\text{in}}} = P_{\text{sun}} - P_{\text{T}} - P_{\text{rad}} - P_{\text{work}} - P_{Q_{\text{out}}}, \qquad (67)$$

because all other terms on the right-hand side have been given above. It can also be evaluated directly inserting the phonon scattering rate in Eq. (C18) (in Appendix C) to the definition in Eq. (56); after some math operation, we have

$$P_{Q_{\text{in}}} = wd_e C_{\text{ph}}^e \int_0^{\epsilon_{\text{cut}}^{\text{ph}}} \epsilon^2 d\epsilon \int_0^\infty dE_e \int_{E_-}^{E_+} (E_e - E') I_{E_e,E'}^{e,\epsilon} dE'$$
$$+ wd_h C_{\text{ph}}^h \int_0^{\epsilon_{\text{cut}}^{\text{ph}}} \epsilon^2 d\epsilon \int_0^\infty dE_h$$
$$\times \int_{E_-}^{E_+} (E_h - E') I_{E_h,E'}^{h,\epsilon} dE', \qquad (68)$$

where

$$I_{E,E'}^{e(h),\epsilon} \equiv \mathcal{A}_{\sqrt{2}\Gamma}(E - E' - \epsilon)\{n_E^{e(h)}[1 - n_{E'}^{e(h)}][1 + f_{0,\beta_{\text{ph}}}^B(\epsilon)]$$
$$- n_{E'}^{e(h)}[1 - n_E^{e(h)}]f_{0,\beta_{\text{ph}}}^B(\epsilon)\}. \qquad (69)$$

$E_{e(h)} - E'$ in the integration of Eq. (68) represents an energy change of the carriers by a phonon scattering event, corresponding to the emitted and absorbed phonon energy. In the limit of zero linewidth ($\Gamma = +0$), Eq. (68) is found to be

$$P_{Q_{\text{in}}} = wd_e C_{\text{ph}}^e \int_0^{\epsilon_{\text{cut}}^{e,-}} \epsilon^3 d\epsilon \int_0^\infty dE_e \{n_{E_e}^e (1 - n_{E_e-\epsilon}^e)$$
$$\times [1 + f_{0,\beta_{\text{ph}}}^B(\epsilon)] - (1 - n_{E_e}^e)n_{E_e-\epsilon}^e f_{0,\beta_{\text{ph}}}^B(\epsilon)\}$$
$$+ wd_h C_{\text{ph}}^h \int_0^{\epsilon_{\text{cut}}^{h,-}} \epsilon^3 d\epsilon \int_0^\infty dE_h \{n_{E_h}^h (1 - n_{E_h-\epsilon}^h)$$
$$\times [1 + f_{0,\beta_{\text{ph}}}^B(\epsilon)] - (1 - n_{E_h}^h)n_{E_h-\epsilon}^h f_{0,\beta_{\text{ph}}}^B(\epsilon)\}, \quad (70)$$

where the terms $\propto \epsilon^3$ in the integrations come from the product of the density of states of LA phonons ($\propto \epsilon^2$) times the phonon energy ϵ. In the simulation shown below, we confirm that $P_{Q_{\text{in}}}$ evaluated by using Eqs. (67) and (68) give the same result (within the numerical accuracy). In this way, total energy current is safely conserved in this theory, as well as the total number current (see the discussion in Sec. III).

G. Numerical method

Simulation results presented in this paper are obtained by numerically finding the steady-state solution of the rate equations for the carrier distribution function in Eqs. (1) and (2) with Eq. (3). Bandwidths of the conduction (electron) and valence (hole) bands are both set to be 10 eV $[0 \leq E_{e(h)} \leq 10 \text{ eV}]$ so that a continuum of the interband transitions covers the whole range of the Sun's spectra for $E > E_g$ (allowing perfect absorption of the above-bandgap photons).

The steady-state solution has been computed by the standard Newton method by discretization of the energy bands. The energy step dE is gradually increased from the bottom of the bands since the carrier distribution function in the steady state is mainly populated near the band bottoms in the whole range of the parameters tested:

$$dE = 0.2 \text{ meV} \quad \text{for } 0 \text{ eV} < E_{e(h)} \leq 0.4 \text{ eV},$$
$$dE = 0.5 \text{ meV} \quad \text{for } 0.4 \text{ eV} < E_{e(h)} \leq 0.6 \text{ eV},$$
$$dE = 1.0 \text{ meV} \quad \text{for } 0.6 \text{ eV} < E_{e(h)} \leq 1.0 \text{ eV},$$
$$dE = 2.0 \text{ meV} \quad \text{for } 1.0 \text{ eV} < E_{e(h)} \leq 2.0 \text{ eV},$$
$$dE = 5.0 \text{ meV} \quad \text{for } 2.0 \text{ eV} < E_{e(h)} \leq 5.0 \text{ eV},$$
$$dE = 10.0 \text{ meV} \quad \text{for } 5.0 \text{ eV} < E_{e(h)} \leq 10.0 \text{ eV}.$$

With these settings, the final results are insensitive to the details of the high-energy cutoff and discretization.

A sequence of iteration of the Newton method converges quickly in this problem, as we find the steady-state solution after several iteration steps in most cases. To validate the numerical results, we also checked numerically that the steady-state solutions satisfy the conservation laws for energy and particle number currents, which must be preserved, in principle, as discussed in Secs. II F and III.

III. BASIC PROPERTIES AND CLASSIFICATION OF THE PARAMETER REGIME

In the previous section, the rate equations that determine the microscopic distribution functions are derived based on our nonequilibrium model. In this section, before we describe the numerical simulation, we give the basic properties related to the particle number conservation laws that must be preserved in any of the steady states for the equations. This information can then be used in the first screening to validate the numerical results obtained. In the latter part of this section, we determine the parameter regime in which the solar cells will work under or out of the detailed balance condition. In this paper, we shall define the latter out-of-equilibrium regime (where the SQ's detailed balance analysis cannot be applied as shown later by the numerical simulation) as the nonequilibrium regime. The parameter regime can be classified from the equation itself without fully solving for it.

A. Conservation of the total number of carriers within the band during phonon scattering processes

The rate equations in Eqs. (1) and (2) represent the net rates for the numbers of particles coming into the microscopic states with energies E_e and E_h. Therefore, as shown in the previous section (Sec. II F), the summation of $dn_{E_{e(h)}}^{e(h)}/dt$ over all microscopic states gives the total net number of electrons (or holes) coming into the absorber (or the cell) per unit time. In the steady state, the net total rate vanishes as a result of the balance between the four terms that are related to generation by sunlight absorption, the radiative recombination loss, extraction to the electrodes, and phonon scattering, on the right-hand side of the rate equation. Among these four terms, the last one, which leads to intraband carrier thermalization, should not change the total number of carriers contained within the band. This basic property must be preserved in our model formulation, which can be checked using the general expression given in Eq. (C18) in Appendix C (with the broadening effect) as shown below.

The net change in the total number of electrons (holes) in the absorber due to the phonon scattering processes per unit time is given by

$$-\mathcal{V}\int_0^\infty \mathcal{D}_{e(h)}[E_{e(h)}]R_{E_{e(h)}}^{e(h),\text{phonon}}dE_{e(h)}. \qquad (71)$$

By inserting Eq. (C18) into Eq. (71), we find that the integrand of the ϵ integration is proportional to

$$\int_0^\infty dE_{e(h)}\int_{E_-}^{E_+}dE'\left[I_{E_{e(h)},E'}^{e(h),\epsilon}-I_{E',E_{e(h)}}^{e(h),\epsilon}\right], \qquad (72)$$

where $I_{E,E'}^{e(h),\epsilon}$ is already defined in Eq. (69).

From the definition of $E_\pm$ given in Eq. (C19) in Appendix C, the integration domain, $E_- < E' < E_+$, is equivalent to

$$E_{e(h)} < \left(\sqrt{E'}+\epsilon\sqrt{\frac{1}{2m_{e(h)}^*v_A^2}}\right)^2, \qquad (73)$$

$$E_{e(h)} > \left(\sqrt{E'}-\epsilon\sqrt{\frac{1}{2m_{e(h)}^*v_A^2}}\right)^2, \qquad (74)$$

which are both symmetrical with respect to the interchange of the following variables: $E' \leftrightarrow E_{e(h)}$. In this way, we find that the two contributions in Eq. (72) cancel perfectly after integration. This ensures that the total number of carriers is preserved within the band during the carrier thermalization process.

B. Conservation of total charge and charge neutrality

The rate equation for the net total charge in the absorber, $Q_{\text{tot}}\{\equiv |e|\sum_k[n_{E_h(k)}^h-n_{E_e(k)}^e]\}$, can also be obtained using the microscopic rate equations. Summation over all states and the difference between those states for the electrons and holes give

$$\frac{d}{dt}Q_{\text{tot}} = -|e|\mathcal{V}\int_0^\infty \mathcal{D}_e(E_e)(R_{E_e}^{e,\text{sun}}-R_{E_e}^{e,\text{rad}}-R_{E_e}^{e,\text{out}})dE_e$$

$$+|e|\mathcal{V}\int_0^\infty \mathcal{D}_h(E_h)(R_{E_h}^{h,\text{sun}}-R_{E_h}^{h,\text{rad}}-R_{E_h}^{h,\text{out}})dE_h, \qquad (75)$$

where the phonon scattering terms are absent, in line with the discussion in Sec. III A. Additionally, the terms for photon absorption and recombination radiation on the right-hand side should all cancel. This should be true because each single-photon absorption and emission process generates or loses one electron-hole pair with no changes in the total charge. This statement can also be verified easily in our formulation using the general expressions for the generation rate [Eq. (7) and (8) for direct gap semiconductors, and Eq. (10) and (11) for indirect

gap semiconductors] and the radiative recombination rate [Eqs. (C11) and (C12) for direct gap semiconductors, and Eqs. (C9) and (C10) for indirect gap semiconductors]. As a result, Eq. (75) can be rewritten as

$$\frac{d}{dt}Q_{\text{tot}} = |e|\mathcal{V}\left[\int_0^\infty \mathcal{D}_e(E_e)R_{E_e}^{e,\text{out}}dE_e\right.$$
$$\left. - \int_0^\infty \mathcal{D}_h(E_h)R_{E_h}^{h,\text{out}}dE_h\right] = 0, \quad (76)$$

where the steady state has been assumed in the second equation. The above equation, which shows that the net extraction rates for the electrons and holes are balanced in the steady state, is used in Eq. (46) in the previous section. Additionally, when using Eqs. (C10) and (C11) along with the definition of the total charge, the total net charge that is present in the absorber is determined from Eq. (70) under steady-state conditions and is given by

$$\frac{Q_{\text{tot}}}{\tau_{\text{out}}} = \frac{|e|\mathcal{V}}{\tau_{\text{out}}}\left[\int_0^\infty \mathcal{D}_h(E_h)\tilde{f}_{-\mu_v,\beta_c}^F(E_h)dE_h\right.$$
$$\left. - \int_0^\infty \mathcal{D}_e(E_e)\tilde{f}_{\mu_c-E_g,\beta_c}^F(E_e)dE_e\right]. \quad (77)$$

From this result, we see that the total charge that is present in the absorber is solely determined by the cell distribution functions (apart from the broadening effect). In the numerical simulations presented here, we focus only on the special case of charge neutrality, where $Q_{\text{tot}} = 0$. When the condition $n_{E_{e(h)}}^{e(h)} \ll 1$ is satisfied at low carrier densities, the charge neutrality condition then relates the chemical potentials in the electrodes, μ_c and μ_v, as follows:

$$\frac{\mu_c + \mu_v}{2} = \frac{E_g}{2} + \frac{\beta_c^{-1}}{2}\ln\frac{d_h}{d_e}. \quad (78)$$

Therefore, using the voltage between the electrodes $(|e|V \equiv \mu_c - \mu_v)$, the chemical potentials can be given by

$$\mu_c = \left[E_g + \beta_c^{-1}\ln(d_h/d_e) + |e|V\right]/2, \quad (79)$$

$$\mu_v = \left[E_g + \beta_c^{-1}\ln(d_h/d_e) - |e|V\right]/2, \quad (80)$$

to enable charge neutrality to be realized in the absorber. In this paper, we set μ_c and μ_v as given in Eqs. (79) and (80).

C. Classification of the parameter regime

In Sec. II, we saw that the rate equation has two characteristic times: τ_{out} for carrier extraction (or time spent in the absorber) and $\tau_{\text{ph}}^{e(h)}$ for carrier thermalization [from Eq. (42)], which will be determinate for the solar-cell properties. As noted in Sec. I, the SQ theory assumes that these two characteristic times should be fast enough for
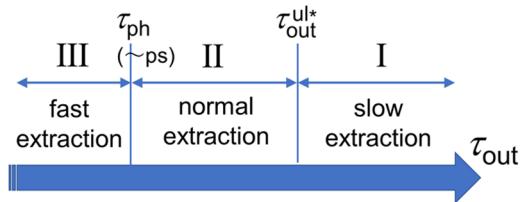

FIG. 8. Classification of parameter space $0 < \tau_{\text{out}} < +\infty$ into three different regimes: (I) slow extraction, where $\tau_{\text{out}} > \tau_{\text{out}}^{\text{ul}*}$; (II) normal extraction, where $\tau_{\text{ph}}^{e(h)} < \tau_{\text{out}} < \tau_{\text{out}}^{\text{ul}*}$; and (III) fast extraction, where $\tau_{\text{out}} < \tau_{\text{ph}}^{e(h)}$.

the detailed balance analysis to be applicable, whereas the quantitative issue of how short these times should be remains to be solved. Here, using the rate equations that are derived using the nonequilibrium approach, we address this issue. In this paper, we shall define a nonequilibrium regime as a parameter regime where the detailed balance analysis cannot be applicable.

In the following discussion, we consider τ_{out} to be a free parameter, while $\tau_{\text{ph}}^{e(h)}$ is the given material parameter and is roughly of picosecond order (although the parameter may be modified to a certain degree by introduction of phononic nanostructures [48,49]). We, therefore, focus on the parameter space given by τ_{out} (in a similar manner to parameterization using the conductance in hot carrier solar cells [6]). As shown in Fig. 8, we divide the parameter space given by $0 < \tau_{\text{out}} < +\infty$ into three different regimes.

In regime III, i.e., the fast extraction regime where $\tau_{\text{out}} < \tau_{\text{ph}}^{e(h)}$, solar-cell operation is likely to be different from that of conventional solar cells because carrier extraction before thermalization with the lattice will become possible [3,4]. In real devices, fast extraction within the ps scale requires an ultrathin absorber. With an average estimated velocity at room temperature of $v_e = \sqrt{2m_e^* \times 3k_B T_c/2} \sim 10^5$ m/s, the carriers can travel a maximum of 0.1 μm within 1 ps. Because the extraction time cannot be less than the travel time from the center of the absorber (where photogeneration occurs) to its surface (where extraction occurs), τ_{out} of less than 1 ps requires absorbers with less than sub-μm thickness in planar solar cells. The situation can hardly be realized in Si solar cells with low-absorption coefficients (a thickness of 10 μm is required even with light trapping for perfect absorption, which is assumed here). To achieve fast extraction in Si solar cells, a meanderlike structure could be used (see Sec. 7.4 in [27]). However, for direct gap semiconductors with higher absorption coefficients, sub-μm-scale absorbers could possibly be used to provide efficient solar cells. This is why hot carrier solar cells should use ultrathin nanostructures with strongly absorbing materials, such as GaAs, as described in the next

section. While we acknowledge these realistic issues, we will however proceed with further discussions and simulation of fast extraction regime III, given that this scenario could even be realized in Si solar cells, to highlight the general properties of solar cells operating in this fast extraction regime.

The SQ theory assumes fast carrier extraction, where the condition $\tau_{\text{out}} < \tau_{\text{ph}}^{e(h)}$ is not required. An upper limit on the extraction time, $\tau_{\text{out}}^{\text{ul}*}[> \tau_{\text{ph}}^{e(h)}]$, should therefore exist, above which the SQ theory will fail to predict the conversion efficiency limit. We can therefore define these two regimes separately using a boundary as the normal extraction regime (II) and the slow extraction regime (I). In regime II, the SQ theory can be used to predict the solar-cell properties. The boundary time $\tau_{\text{out}}^{\text{ul}*}$ between regimes I and II, which will be dependent on device parameters such as the material and thickness of the absorber, can be evaluated as shown in the remainder of this section.

In regimes I and II, we can safely assume that the thermalization (intraband carrier cooling) is completed within the absorber because the phonon scattering rate dominates the other terms in the rate equations, Eqs. (1) and (2). In this case, the carrier distribution function in the cell is given by the Fermi-Dirac distribution function in Eq. (46), while the chemical potentials in the cell can differ from those in the electrodes, i.e., $\mu_{e(h)}^{\text{cell}} \neq \mu_{e(h)}$. When the function in Eq. (46) has been assumed, we can insert $-R_{E_{e(h)}}^{e(h),\text{phonon}} = 0$ into the rate equations in Eqs. (1) and (2). This is what we observed earlier in Sec. II E.

We should also reconsider the meaning of the relation $\mu_{e(h)}^{\text{cell}} \neq \mu_{e(h)}$ here. This means that the carrier distribution functions in the cell differ from those in the electrodes, while they are assumed to be equal in the SQ theory when calculating the radiative recombination loss. Using the difference $\Delta n_{E_{e(h)}}^{e(h)} \{\equiv n_{E_{e(h)}}^{e(h)} - f_{\mu_{e(h)},\beta_c}^F[E_{e(h)}]\}$, the microscopic rate equations for the steady states can be rewritten as

$$R_{E_{e(h)}}^{e(h),\text{out}} = \frac{\Delta n_{E_{e(h)}}^{e(h)}}{\tau_{\text{out}}} = R_{E_{e(h)}}^{e(h),\text{sun}} - R_{E_{e(h)}}^{e(h),\text{rad}}. \quad (81)$$

Therefore, the difference is given by

$$\Delta n_{E_{e(h)}}^{e(h)} = \tau_{\text{out}} \left[R_{E_{e(h)}}^{e(h),\text{sun}} - R_{E_{e(h)}}^{e(h),\text{rad}} \right]$$
$$\approx \tau_{\text{out}} R_{E_{e(h)}}^{e(h),\text{sun}}, \quad (82)$$

where, in the second line, we use the approximation $R_{E_{e(h)}}^{e(h),\text{sun}} \gg R_{E_{e(h)}}^{e(h),\text{rad}}$, which is usually fulfilled at the maximum operating power point of $V = V_{\text{mp}}^{\text{eq}}$ (0.779 V for Si and 1.052 V for GaAs at 1 sun when using our 6000-K blackbody sun), being focused from this point in this subsection. Now we will determine the condition by which the SQ conversion efficiency limit can be modified. When τ_{out}

increases inside regime II and gradually approaches I, we can fix the maximum operating power point because the maximum power condition given in the SQ theory will at least remain unchanged inside regime II. The SQ calculation using $n_{E_{e(h)}}^{e(h)} = f_{\mu_{e(h)},\beta_c}^F[E_{e(h)}]$ will be justified as long as $\Delta n_{E_{e(h)}}^{e(h)} \ll f_{\mu_{e(h)},\beta_c}^F[E_{e(h)}]$ is satisfied at $V = V_{\text{mp}}^{\text{eq}}$, which can be read as

$$\tau_{\text{out}} \ll \frac{f_{\mu_{e(h)},\beta_c}^F[E_{e(h)}]}{R_{E_{e(h)}}^{e(h),\text{sun}}} \equiv \tau_{\text{out}}^{\text{ul}}[E_{e(h)}]. \quad (83)$$

When $\tau_{\text{out}} > \tau_{\text{out}}^{\text{ul}}[E_{e(h)}]$, the conversion efficiency limit can then differ from the limit from the SQ theory. A sufficient condition for the SQ calculation to be justified is that where Eq. (83) is fulfilled over an energy range in which there is a non-negligible carrier distribution that makes a relevant contribution to the radiative recombination; this is given approximately by $0 < E_{e(h)} < k_B T_c$. {Given that $f_{\mu_{e(h)},\beta_c}^F[E_{e(h)}]$ decreases exponentially with $E_{e(h)}$, it is almost impossible to satisfy this condition at higher energies.} In this way, the upper boundary of parameter regime II can be evaluated, in principle, using $\tau_{\text{out}}^{\text{ul}}[E_{e(h)}]$ in Eq. (83), e.g., by selecting $E_{e(h)} = k_B T_c$ as a typical carrier energy scale.

In Fig. 9, we plotted the boundary time $\tau_{\text{out}}^{\text{ul}*}$ that is defined using 10% of $\tau_{\text{out}}^{\text{ul}}(E_e = k_B T_c)$ as a function of absorber thickness w for Si and GaAs solar cells. Figure 9(a) clearly shows that $\tau_{\text{out}}^{\text{ul}*}$ is dependent on the material parameters (effective mass and indirect or direct gap) and is linearly on w. For 100-μm-thick Si solar cells, $\tau_{\text{out}}^{\text{ul}*}$ is estimated to be on the sub-ms scale. Additionally, $\tau_{\text{out}}^{\text{ul}*}$ will decrease in the concentrator solar cells and is plotted as a function of concentration ratio $\mathcal{CR}$ in Fig. 9(b). $\tau_{\text{out}}^{\text{ul}*}$ is roughly proportional to $1/\sqrt{\mathcal{CR}}$.

The physical meaning of this condition still seems unclear since $\tau_{\text{out}}^{\text{ul}}[E_{e(h)}]$ in Eq. (83) is dependent on energies of the microscopic carrier states. The physical meaning of the time scale will become clearer if the condition $\Delta n_{E_{e(h)}}^{e(h)} \ll f_{\mu_{e(h)},\beta_c}^F[E_{e(h)}]$ is summed over all the microscopic states. This can be read as

$$\tau_{\text{out}} \ll \frac{\mathcal{V} \int \mathcal{D}_{e(h)}[E_{e(h)}] f_{\mu_{e(h)},\beta_c}^F[E_{e(h)}] dE_{e(h)}}{\mathcal{V} \int \mathcal{D}_{e(h)}[E_{e(h)}] R_{E_{e(h)}}^{e(h),\text{sun}} dE_{e(h)}}$$
$$\approx \frac{N_c}{I_{\text{sc}}^{\max}/|e|} \left(= \frac{n_c}{i_{\text{sc}}^{\max}/|e|} \times w \right), \quad (84)$$

where $N_c (= N_e = N_h)$ is the total number of carriers, $n_c \equiv N_c/\mathcal{V}$ is the carrier density (where $n_c w = N_c/\mathcal{A}$ is the areal density); the maximum available short-circuit current $I_{\text{sc}}^{\max}$ is given by

$$I_{\text{sc}}^{\max} \equiv |e| \times \mathcal{A} \times \int_{E_g}^{\infty} j^{\text{sun}}(E)E, \quad (85)$$
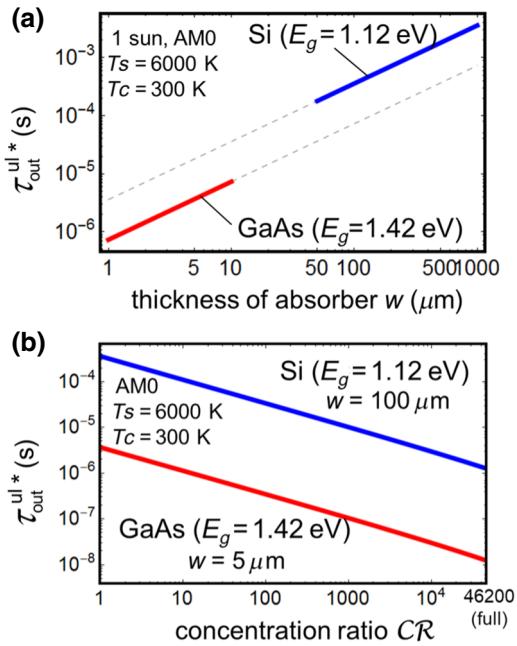
FIG. 9. Upper boundary of the extraction time $\tau_{\mathrm{out}}^{\mathrm{ul}*}$ when evaluated as 10 percent of $\tau_{\mathrm{out}}^{\mathrm{ul}}(E_e = k_B T_c)$ in Eq. (83), shown as functions of (a) cell thickness w and (b) the concentration ratio for planar Si and GaAs solar cells. In (a), we assume 1-sun illumination ($\mathcal{CR} = 1$) and maximum power operation at $V = V_{\mathrm{mp}}^{\mathrm{eq}}$ (=0.779 V for Si and 1.052 V for GaAs). In (b), the absorber thickness w is fixed at 100 μm for Si and 5 μm for the GaAs cells. The $\mathcal{CR}$ dependence of $V_{\mathrm{mp}}^{\mathrm{eq}}(\mathcal{CR})$ is calculated using the SQ theory.

from which the corresponding current density per unit area is defined using

$$i_{\mathrm{sc}}^{\mathrm{max}} = I_{\mathrm{sc}}^{\mathrm{max}}/\mathcal{A}. \tag{86}$$

The meaning of the condition in Eq. (84), which is equivalent to $N_c/\tau_{\mathrm{out}} \gg I_{\mathrm{sc}}^{\mathrm{max}}/|e|$, is now much clearer. The number of carriers output from the absorber per unit time (which differs from the net current given by the outflow minus the inflow) must be greater than the number of photons absorbed per unit time, i.e., the number of carriers that is generated per unit time in the absorber. This condition may have simply been assumed in the SQ theory, although it is not given explicitly in their original paper [1].

The final equation in Eq. (84) clearly explains the w-linear dependence of $\tau_{\mathrm{out}}^{\mathrm{ul}*}$ shown in Fig. 9(a). Note here that $i_{\mathrm{sc}}^{\mathrm{max}}$ and the carrier density n_c are independent of w because $i_{\mathrm{sc}}^{\mathrm{max}}$ is given solely by the sun-illumination conditions and n_c is given by the chemical potential that is fixed at the maximum operating power point, $V = V_{\mathrm{mp}}^{\mathrm{eq}}$. The $\mathcal{CR}$ dependence of $\tau_{\mathrm{out}}^{\mathrm{ul}*} \propto 1/\sqrt{\mathcal{CR}}$ shown by Fig. 9(b) can also be understood based on the following analysis. The radiative loss current I_{rad} at the maximum operating power can be estimated from the SQ theory using the I-V relation, where $I = I_{\mathrm{sun}} - I_{\mathrm{rad}}$ with $I_{\mathrm{rad}} = I_{\mathrm{rad}}^0(e^{\beta_c|e|V} - 1) \approx$

$I_{\mathrm{rad}}^0 e^{\beta_c|e|V}$ (see Sec. I). Using $d(IV)/dV = 0$, we can easily show that $I_{\mathrm{rad}} \approx I_{\mathrm{sun}}/(\beta_c V_{\mathrm{mp}}^{\mathrm{eq}})$ as long as $\beta_c V_{\mathrm{mp}}^{\mathrm{eq}} \gg 1$, which is normally fulfilled. In general, $V_{\mathrm{mp}}^{\mathrm{eq}}$ increases with the concentration ratio $\mathcal{CR}$; at the same time, however, it can never exceed the absorber band gap E_g for solar-cell operation (below the lasing condition [50]), i.e., $V_{\mathrm{mp}}(\mathcal{CR} = 1) \leq V_{\mathrm{mp}}(\mathcal{CR}) \leq E_g$. In Si, for example, this means that 0.779 eV $\leq V_{\mathrm{mp}}^{\mathrm{eq}}(\mathcal{CR}) \leq 1.12$ eV, and correspondingly, $I_{\mathrm{rad}} \left[\approx I_{\mathrm{sun}}/(\beta_c V_{\mathrm{mp}}^{\mathrm{eq}})\right]$ ranges at most from 2.3 to 3.3 percent of I_{sun} over the whole $\mathcal{CR}$ range $[1 \leq \mathcal{CR} \leq 46\,200$ (full)]. Therefore, I_{rad} is almost proportional to $I_{\mathrm{sun}}(\propto \mathcal{CR})$. In addition, we notice that the radiative loss current in general is $I_{\mathrm{rad}} \propto n_c^2$, or equivalently, $n_c \propto I_{\mathrm{rad}}^{1/2} \propto \mathcal{CR}^{1/2}$. Because $i_{\mathrm{sc}}^{\mathrm{max}}$ is obviously $\propto I_{\mathrm{sun}} \propto \mathcal{CR}$, another definition of $\tau_{\mathrm{out}}^{\mathrm{ul}*}$ from Eq. (84) shows that $\tau_{\mathrm{out}}^{\mathrm{ul}*} \propto n_c/i_{\mathrm{sc}}^{\mathrm{max}} \propto \mathcal{CR}^{-1/2}$.

D. Carrier distribution function in the three regimes

In this subsection, we will show the carrier distribution function in the steady state, $n_{E_e}^e$, obtained by fully solving the rate equations, in Eqs. (1) and (2), in three regimes of τ_{out}, which is introduced in Sec. III C. In Sec. III C, we classify the regime of τ_{out}, in terms of the maximum conversion efficiency. Thus, in finding the upper boundary $\tau_{\mathrm{out}}^{\mathrm{ul}*}$, we concentrate the distribution functions at $V = V_{\mathrm{mp}}^{\mathrm{eq}}$, the max power point voltage in the SQ theory (in regime II). Here we will see the dependence on V as well.

Figure 10 shows the electron distribution functions for different τ_{out} [$= 10^{-2}, 10^{-8}, 10^{-13.5}, 10^{-14.5}$ s] at different bias voltages, $|e|V$: (a) $|e|V_{\mathrm{oc}}^{\mathrm{eq}}$ (=0.868 eV), (b) $0.5E_g$, (c) $0.1E_g$, and (d) $0.01E_g$]. For parameters (τ_{out}, V) belongs to three different regimes (I, II, III) in Fig. 10(e), the steady-state distribution functions have different characteristics, which are summarized as follows:

Regime II (quasi equilibrium regime): The distribution function (black curves) smoothly connects two asymptotic expressions between low and high energies;

$$n_{E_e}^e = f_{\mu_c,\beta_c}^F(E_g + E_e), \tag{87}$$

for low energy (line A, dashed), and

$$n_{E_e}^e = \tau_{\mathrm{ph}}^e(E_e) \times R_{E_e}^{e,\mathrm{sun}} \tag{88}$$

for high energy (line B, dotted), where the high-energy expression for the phonon-relaxation time is given by

$$\left[\tau_{\mathrm{ph}}^e(E_e)\right]^{-1} = \frac{C_{\mathrm{ph}}^e}{\sqrt{E_e}} \times \beta_S \times \frac{(\epsilon_{\mathrm{cut}}^{\mathrm{ph}})^4}{4}. \tag{89}$$

Regime I: The distribution function (blue curves) has a low-energy asymptotic form, $n_{E_e}^e = f_{\mu_c^{\mathrm{cell}},\beta_c}^F(E_g + E_e)$ with $\mu_c^{\mathrm{cell}} > \mu_c$, thus lies above line A (for the same reason presented in Sec. III C), whereas the high-energy asymptotic form is the same as that in regime II (line B).

Regime III: The distribution function (red and magenta curves) has a high-energy asymptotic form

$$n_{E_e}^e = \tau_{\text{out}} \times R_{E_e}^{e,\text{sun}} \qquad (90)$$

(line C, dot-dashed), which decreases with decreasing τ_{out} and lies below line B considering $\tau_{\text{out}} < \tau_{\text{ph}}^e$ in regime III. The low-energy asymptotic form depends also on τ_{out}. While it is given by $n_{E_e}^e = f_{\mu_c,\beta_c}^F(E_g + E_e)$ (line A) for the slower extraction [10^{-14} s $< \tau_{\text{out}} < \tau_{\text{ph}}^e$ in Fig. 10(e)], it is given by $n_{E_e}^e = f_{\mu_c^{\text{cell}},\beta_c}^F(E_g + E_e)$ with $\mu_c^{\text{cell}} > \mu_c$ for the faster extraction ($\tau_{\text{out}} < 10^{-14}$ s) and lies above line A. In the latter case, the increase in the carrier temperature is also observed (for the intermediate energies), and thus the distribution functions largely deviate from those obtained in regime II.

The boundary between regime I and regime II is where the chemical potential μ_c^{cell} starts to deviate from that in the electrode μ_c, and thus can be determined by the same argument as presented in Sec. III C. Therefore, the boundary, $\tau_{\text{out}} = \tau_{\text{out}}^{\text{ul}}(\equiv f_{\mu_c,\beta_c}^F(E_g + E_e)/R_{E_e}^{e,\text{sun}})$ displayed in Fig. 10(e) is now dependent on the voltage V, which enters through μ_c in $f_{\mu_c,\beta_c}^F(E_g + E_e)$.

The high-energy tails, line B in regimes I and II, and line C in regime III, are explained by the following analysis. In the high-energy limit, the rate equation, Eq. (1) for the steady state, is rewritten as

$$R_{E_e}^{e,\text{sun}} + \frac{\tilde{f}_{\mu_c,\beta_c}(E_g + E_e)}{\tau_{\text{out}}} - \left[\frac{1}{\tau_{\text{out}}} + \frac{1}{\tau_{\text{ph}}^e(E_e)}\right] n_{E_e}^e$$

$$\approx R_{E_e}^{e,\text{sun}} - \left[\frac{1}{\tau_{\text{out}}} + \frac{1}{\tau_{\text{ph}}^e(E_e)}\right] n_{E_e}^e$$

$$= 0, \qquad (91)$$

where we neglect the radiation loss term $R_{E_e}^{e,\text{rad}}$ (smaller than $R_{E_e}^{e,\text{sun}}$). We also use an approximation $R_{E_e}^{e,\text{phonon}} \approx n_{E_e}^e/\tau_{\text{ph}}^e(E_e)$ with the phonon relaxation time given in Eq. (89), which is obtained by inserting $n_{E_e}^e \propto e^{-\beta_s E_e}$ in $R_{E_e}^{e,\text{phonon}}$ in Eq. (B8). In the left-hand side of the first equation, we further use a fact that the second term responsible for injection from the electrode ($\propto e^{-\beta_c E_e}$) is much smaller than the first generation term $R_{E_e}^{e,\text{sun}}(\propto e^{-\beta_s E_e})$ and can be dropped at high energy. With Eq. (91), we find the asymptotic expressions for line B and line C: Eq. (88) for $\tau_{\text{out}} \gg \tau_{\text{ph}}^e(E_e)$, and Eq. (90) for $\tau_{\text{out}} \ll \tau_{\text{ph}}^e(E_e)$.

Presence of the high-energy tail ($n_{E_e}^e \propto R_{E_e}^{e,\text{sun}} \propto e^{-\beta_s E_e}$) clearly shows that residual high-energy population cannot be removed perfectly from the absorber due to finite time scales required for carrier extraction and carrier cooling (phonon emission). The high-energy residual population [$< \tau_{\text{ph}}^e(E_e) \times R_{E_e}^{e,\text{sun}}$] is very small and will not affect
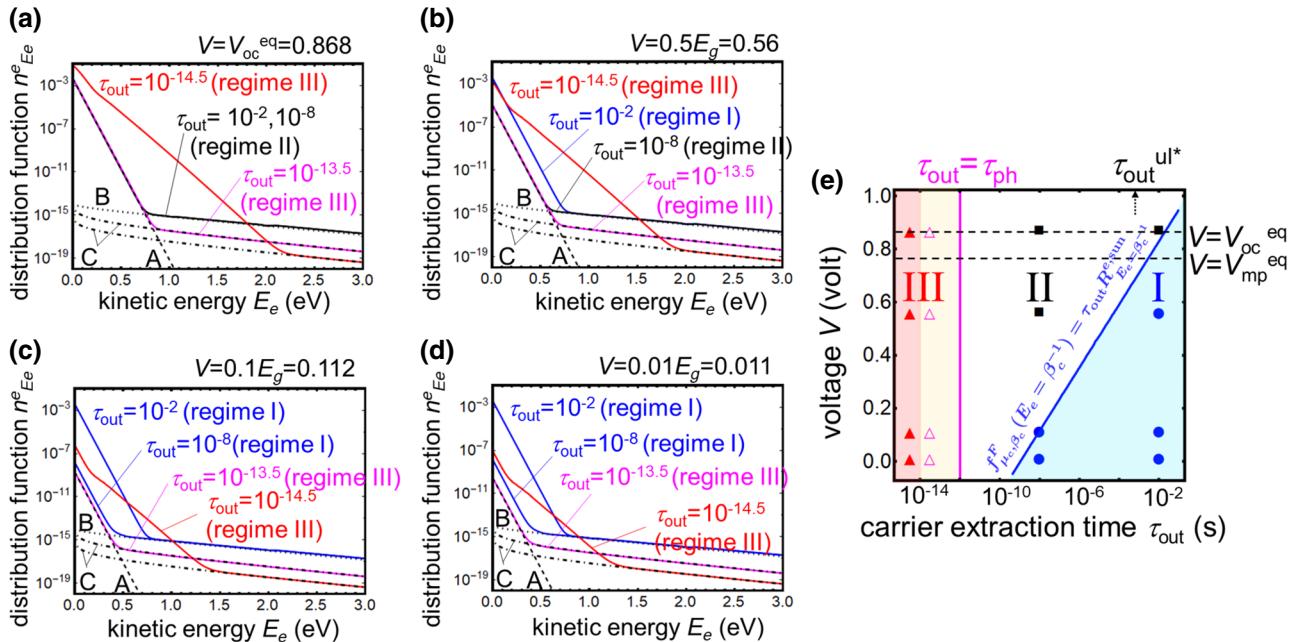
FIG. 10. Carrier (electron) distribution functions in the absorber for different $\tau_{\text{out}}(= 10^{-2}, 10^{-8}, 10^{-13.5}, 10^{-14.5}$ s) and at different bias voltages $|e|V$: (a) $|e|V_{\text{oc}}^{\text{eq}}$ (=0.868 eV), (b) $0.5E_g$, (c) $0.1E_g$, and (d) $0.01E_g$. In (e), the parameter space (τ_{out}, V) is classified into the tree regimes where the distribution functions have different characters (see the text for details). Simulations are performed for simple planar solar cell with a 100-μm-thick Si absorber at 1 sun ($\mathcal{CR} = 1$) with a 6000-K blackbody spectrum.

macroscopic quantity in normal cases unless the phonon relaxation time τ_{ph} is prolonged (e.g., by using the phonon bottleneck effect in hot carrier solar-cell absorbers with carrier confinement and/or phononic crystals [51]) and the illumination is very strong with large $\mathcal{CR}$.

IV. NUMERICAL SIMULATION OF DEVICE PERFORMANCE AND THE CONVERSION EFFICIENCY LIMIT OF A SIMPLE PLANAR SOLAR CELL

In this section, we present numerical simulation results for the device performance and the conversion efficiency limit of a simple planar solar cell. The results obtained here are summarized in Fig. 11, which shows the theoretical conversion efficiency limit as a function of carrier extraction time τ_{out} for various values of concentration ratio $\mathcal{CR}$. As shown in Fig. 11, two curves (solid and dashed lines) are presented for a given $\mathcal{CR}$. The theoretical limit is dependent on how effectively the heat that is generated in the crystal lattices of the absorber and the electrodes can be delivered to each other via phonon transport. In the ideal limit case, where phonon transport between the absorber and the electrodes is very fast in either direct or indirect ways, which we shall refer to as heat-shared phonon reservoirs [see Fig. 12(a)], we have higher maximum conversion efficiencies (shown as solid curves in Fig. 11) when the carrier extraction becomes fast. At the opposite limit, where the phonon transport between absorber and electrodes so slow as to be negligible, which we refer to as heat-isolated phonon reservoirs [Fig. 12(b)], the maximum conversion efficiency is reduced when the carrier extraction becomes fast (see the dashed curves in
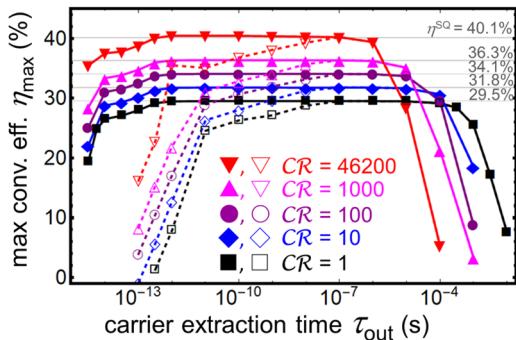
FIG. 11. Summary of device simulation results for a simple planar solar cell with a 100-μm-thick Si absorber using our nonequilibrium theory; the maximum conversion efficiency is shown as a function of carrier extraction time τ_{out} for various concentration ratios ($\mathcal{CR} = 1, 10^1, 10^2, 10^3, 46\,200$). The solid lines are obtained for the heat-shared phonon reservoirs and the dashed lines are obtained for the heat-isolated phonon reservoirs (as explained in the text). The realistic limit for the maximum efficiency will lie between the solid and dashed curves. The SQ limit for each $\mathcal{CR}$ is also indicated using horizontal lines.
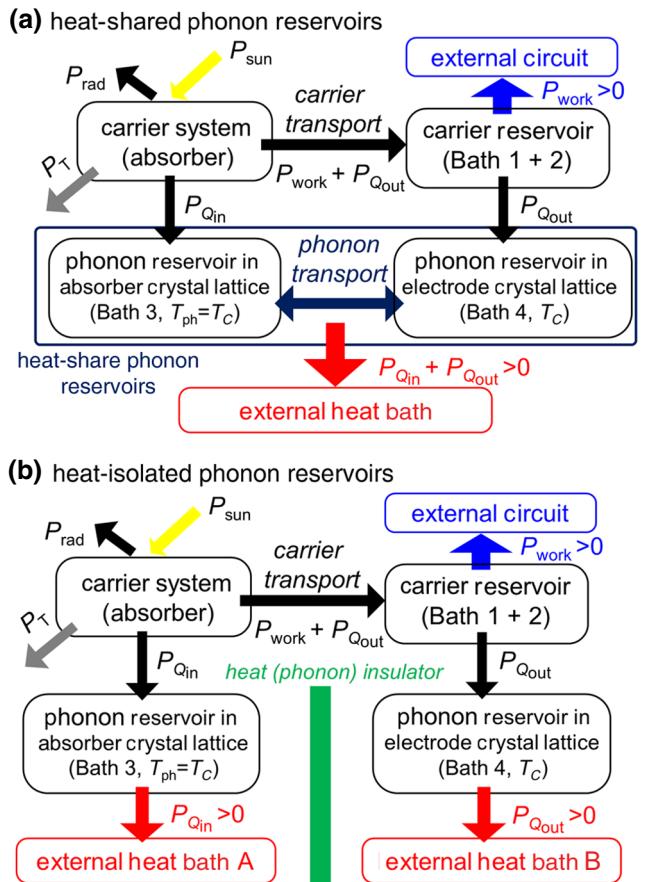
FIG. 12. Two ideal models that take the phonon environments in the two limiting cases into account: (a) heat-shared phonon reservoirs, where the phonon transport between the absorber and electrodes is very fast, in either direct or indirect ways; and (b) heat-isolated phonon reservoirs, where the phonon transport between the absorber and electrodes is very slow. In the latter case, the heat generated in the absorber ($P_{Q_{in}}$) and in the electrodes ($P_{Q_{out}}$) are dissipated independently into different heat baths (heat baths A and B). To enable solar-cell operation, $P_{work} > 0$ must be self-sustained solely by solar illumination $P_{sun} > 0$; the requirements are that $P_{Q_{in}} + P_{Q_{out}} > 0$ for (a) heat-shared phonon reservoirs, and that $P_{Q_{in}} > 0$ and $P_{Q_{out}} > 0$ for (b) the heat-isolated phonon reservoirs. Otherwise, an additional external heat supply to the absorber and/or the electrodes will be required to sustain solar-cell operation; the definition of the solar-cell conversion efficiency then becomes less clear.

Fig. 11). In realistic cases, the maximum conversion efficiency will lie somewhere between these two curves. The precise position will be dependent on the phonon transport properties between the absorber and the electrodes, which will be sensitive to the formation conditions for the contacts between the absorber and the electrodes and/or the phonon environment surrounding them.

The differences in the two ideal cases are incorporated into the stability conditions for solar-cell operation. To enable solar-cell operation with $P_{work} > 0$ to be

self-sustained solely by solar illumination with $P_{\text{sun}} > 0$, the requirements are that $P_{Q_{\text{in}}} + P_{Q_{\text{out}}} > 0$ for the heat-shared phonon reservoirs shown in Fig. 12(a), and that $P_{Q_{\text{in}}} > 0$ and $P_{Q_{\text{out}}} > 0$ for the heat-isolated phonon reservoirs shown in Fig. 12(b). Otherwise, an additional external heat supply to the absorber and/or the electrodes will be required to sustain solar-cell operation, and the definition of the solar-cell conversion efficiency then becomes less clear. In the following subsections, we discuss the solar-cell properties and the underlying physics for these two limiting cases.

A. A limiting case: heat-shared phonon reservoirs

We now present numerical simulation results for a limiting case involving heat-shared phonon reservoirs. The solid lines in Fig. 11 show the maximum conversion efficiencies for various concentration ratios ($\mathcal{CR} = 1, 10, 10^2, 10^3, 46\,200$) plotted as a function of the carrier extraction time τ_{out}. We find flat regions for τ_{out} of more than 1 ps and less than $\tau_{\text{out}}^{\text{ul*}}$, which is dependent on the concentration ratio $\mathcal{CR}$ [Fig. 9(b)], while the maximum conversion efficiency is equal to the SQ limit η^{SQ}. As expected, we can conclude that the SQ theory applies in the normal extraction regime II. Outside this regime, in both the slow and fast extraction regimes denoted by I and III, respectively, we find significant reductions in η_{max} for the simple planar solar cell (Fig. 3). Because the solar-cell properties are different for each regime, our definition of the parameter classifications in Fig. 8 seems reasonable. We must now consider how the difference can be understood.

Figure 13 shows an increase in the Fermi levels of the electrons and holes in the absorber when compared with those in the electrodes, denoted by $\Delta\mu_e \equiv \mu_c^{\text{cell}} - \mu_c$ and $\Delta\mu_h \equiv (-\mu_v^{\text{cell}}) - (-\mu_v)$, respectively, when evaluated using the carrier distribution functions at the maximum operating power point $V = V_{\text{mp}}$ under 1-sun illumination ($\mathcal{CR} = 1$). The increases in the Fermi levels found in regimes I and III clearly show that the carriers in the absorber form nonequilibrium populations. We checked numerically that similar results are also obtained for higher values of concentration ratio $\mathcal{CR} > 1$. The increased Fermi levels in the different regimes originate from different mechanisms. In regime I, the carriers are accumulated in the absorber because of the slow extraction process, resulting in increases in the carrier density and Fermi level. In contrast, the increment in regime III is attributed to broadening of the microscopic states because $\Gamma = \hbar/\left(2\sqrt{\log 2}\,\tau_{\text{out}}\right)$ is no longer negligible. In this regime, the dominant term in the rate equation is the carrier extraction term $R_{E_{e(h)}}^{e(h),\text{out}}$, which allows us to have $R_{E_{e(h)}}^{e(h),\text{out}} \approx 0$. As a result, the carrier distribution functions in the absorber can be approximated using $n_{E_e}^e \approx \tilde{f}_{\mu_c,\beta_c}^F(E_g + E_e)$
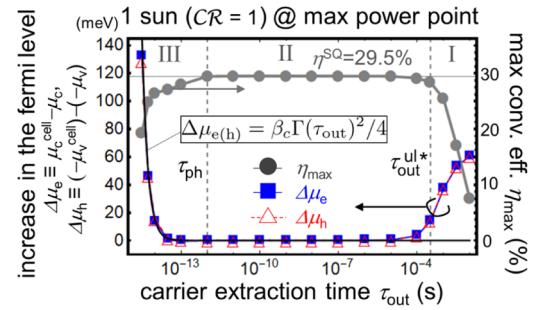
FIG. 13. Increases in the Fermi levels of electrons and holes in the absorber when compared with that in the electrodes; $\Delta\mu_e \equiv \mu_c^{\text{cell}} - \mu_c$ and $\Delta\mu_h \equiv (-\mu_v^{\text{cell}}) - (-\mu_v)$ are evaluated at the maximum operating power point $V = V_{\text{mp}}$ and are shown as functions of carrier extraction time (for 100-μm-thick Si under 1-sun-AM0 illumination). The maximum conversion efficiency (the black solid line shown in Fig. 11) is also shown.

and $n_{E_h}^h \approx \tilde{f}_{-\mu_v,\beta_c}^F(E_h)$ from Eq. (C13) and (C14). As long as the band-filling effect remains negligible, i.e., when $n_{E_e}^e \ll 1$ and $n_{E_h}^h \ll 1$, the distribution functions from Eq. (C12) can be approximated using

$$n_{E_e}^e \approx \exp\{-\beta_c[E_g + E_e - (\mu_c + \beta_c\Gamma^2/4)]\}, \quad (92)$$

$$n_{E_h}^h \approx \exp\{-\beta_c[E_h - (-\mu_v + \beta_c\Gamma^2/4)]\}. \quad (93)$$

Therefore, in this regime, the increases in the Fermi levels are fitted well using

$$\Delta\mu_e \equiv \mu_c^{\text{cell}} - \mu_c \approx \beta_c\Gamma^2/4, \quad (94)$$

$$\Delta\mu_h \equiv (-\mu_v^{\text{cell}}) - (-\mu_v) \approx \beta_c\Gamma^2/4. \quad (95)$$

To see what happens in the nonequilibrium regimes directly, we simulate the energy balance at the maximum operating power point, as shown in Fig. 14, which provides further information on the energy-loss mechanism. In slow extraction regime I, the energy loss caused by radiative recombination (P_{rad}) increases greatly with increasing τ_{out}, while that due to thermal loss ($P_{Q_{\text{in}}} + P_{Q_{\text{out}}}$) decreases. This can be understood easily because the slow extraction process increases the carrier density in the absorber, which thus enhances the radiative recombination rate. In contrast, in fast extraction regime III in Fig. 14, the thermal loss $P_{Q_{\text{in}}} + P_{Q_{\text{out}}}$ increases as τ_{out} decreases, whereas P_{rad} is almost unchanged. In this regime, the output power P_{work} decreases as τ_{out} decreases. These results can be explained by a reduction in the output voltage (as will be evidenced in Fig. 15), which increases excess heat carried by a pair of electron and hole extracted to the electrodes. We would like to remark that, as shown in Fig. 14, the requirement for stable solar-cell operation, given by $P_{Q_{\text{in}}} + P_{Q_{\text{out}}} > 0$ in this model with heat-shared phonon reservoirs, is fulfilled
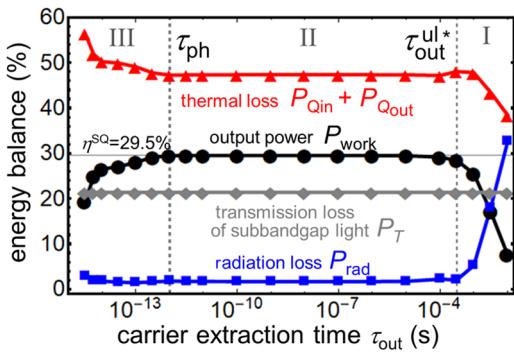
FIG. 14. Energy balance evaluated at the maximum operating power point $V = V_{mp}$ as a function of carrier extraction time (100-μm-thick Si under 1-sun-AM0 illumination).

(and is also fulfilled for $0 < V < V_{oc}$, which is not shown here).

The differences between these loss mechanisms are reflected in their current-voltage (I-V) characteristics in each regime, as shown in Fig. 15. In slow extraction regime I [Fig. 15(a)], the short-circuit current I_{sc} decreases with increasing τ_{out} while the open-circuit voltage V_{oc} remains unchanged. In contrast, in fast extraction regime
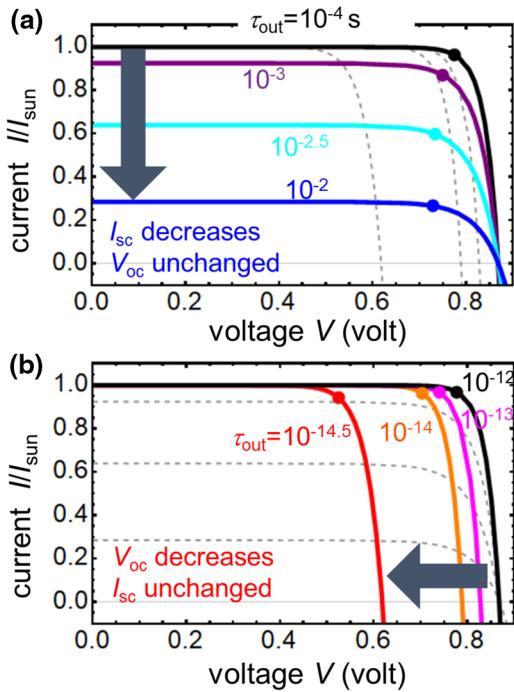
FIG. 15. Current-voltage characteristics for various carrier extraction times (100-μm-thick Si under 1-sun-AM0 illumination): (a) curves obtained in slow extraction regime I are highlighted; (b) curves obtained in fast extraction regime III are highlighted. The max power points are indicated on each curves by filled circles. The solid black curves in (a) and (b) are obtained for 10^{-12}s $\leq \tau_{out} \leq 10^{-4}$s in normal extraction regime II.

III [Fig. 15(b)], the open-circuit voltage V_{oc} decreases with decreasing τ_{out} while the short-circuit current I_{sc} remains unchanged. These results agree with the consideration that, at least at the max power voltage (on filled circles in Fig. 15), while the enhanced radiation loss in regime I in Fig. 14 accompanies a significant loss in the output charge current, the enhanced heat dissipation in regime III in Fig. 14 does not necessarily require significant charge-current loss. We find no significant changes in the I-V characteristics for τ_{out} between 1 ps and $10^{-3.5}$ s, thus supporting the belief that the SQ theory works in normal extraction regime II.

Reduction in V_{oc} in the fast extraction regime III can be analyzed further by monitoring the radiation current loss I_{rad} and the nonequilibrium distribution function as a function of τ_{out} at a given voltage (say $V = V_{oc}^{eq} \approx 0.868$ V, an open-circuit voltage in normal extraction regime II). In Fig. 16(a), we find the reduction in the open-circuit voltage $-\Delta V_{oc} (\equiv V_{oc} - V_{oc}^{eq})$ follows $\Delta V_{oc} = \beta_c \Gamma^2/2$ for $\tau_{out} < 10^{-14}$. However, we can see the reduction already starts to appear from the slower extraction $10^{-14} < \tau_{out} < 10^{-12}$. Accordingly, an increase in the radiation current loss I_{rad} is found for the same range $\tau_{out} < 10^{-12}$ in Fig. 16(b). The results show that, in regime III, there is another factor of reducing output current, which is not directly related to the population change. To depict the physics behind, we plotted in Fig. 16(b) two factors, a population enhancement factor $\mathcal{F} = \exp(\beta_c \Gamma^2/2)$ by a dotted line, and a spectral reshaping factor by a dashed line,

$$ S(\Gamma) = \frac{\int_0^\infty E_{eh}^2 \Theta\left(\frac{E_g}{\sqrt{2}\Gamma}, \frac{E_{eh}}{\sqrt{2}\Gamma}\right) e^{-\beta_c E_{eh}} dE_{eh}}{\int_0^\infty (E_g + E_{eh})^2 e^{-\beta_c E_{eh}} dE_{eh}}, \qquad (96) $$

which accounts for the reshaping and redshift of the emission spectra [$\Theta(x, y)$ is defined in Appendix C]. Now it becomes much clearer that the enhancement in I_{rad} is mainly due to the spectral reshaping factor S in the slower extraction regime $10^{-14} < \tau_{out} < 10^{-12}$, whereas a sharp increase for $\tau_{out} < 10^{-14}$ is due to the population enhancement factor $\mathcal{F}$. Thus, overall τ_{out} dependency can be explained by their product $S \times \mathcal{F}$ (solid line). Figure 16(c) shows the electron distribution function for different τ_{out} in regime III for the fixed voltage, $V = V_{oc}^{eq} \approx 0.868$ V. A large increase in the population found only for $\tau_{out} < 10^{-14}$ is consistent with the above discussion on the radiation current loss.

Our results are consistent with the results obtained by NEGF theory for a nanostructured solar cell containing a finite number of quantum dots [52]. Reduction in the carrier extraction efficiency found for weak interdot and dot-contact couplings (in Fig. 15 of [52]) corresponds to the reduction of I_{sc} found in regime I in our model. The broadening-induced degradation effect in the fast
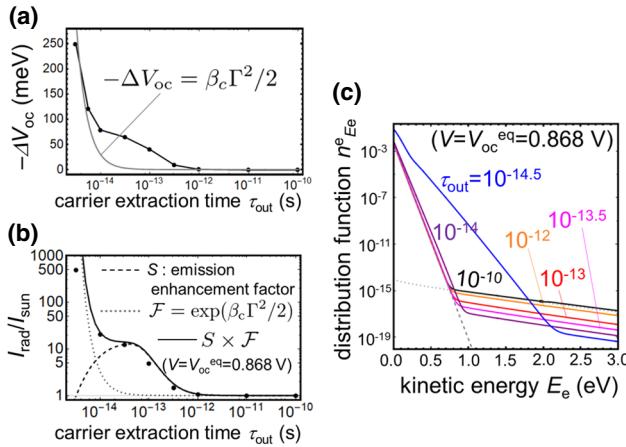
FIG. 16. (a) Reduction in the open-circuit voltage $-\Delta V_{\text{oc}}(\equiv V_{\text{oc}}^{\text{eq}} - V_{\text{oc}})$, and (b) the radiative current loss $I_{\text{rad}}/I_{\text{sun}}$ at $V = V_{\text{oc}}^{\text{eq}} = 0.868$ V are plotted as a function of τ_{out} in the fast extraction regime III. (c) Nonequilibrium electron distribution function at $V = V_{\text{oc}}^{\text{eq}} = 0.868$ V is plotted for different τ_{out} in regime III (100-μm-thick Si under 1-sun-AM0 illumination).

extraction regime in our model can be understood alternatively as effective bandgap narrowing [$E_g \rightarrow E_g^{\text{eff}}(= E_g - \beta_c\Gamma^2/2)$], by which the open-circuit voltage should be reduced. Similar subbandgap states are also found in their NEGF study [52], whereas their spacially resolved theory (different from ours) tells that modification in the local density of states below the band edge is found only in the vicinity of contacts. By seeing the difference, we speculate that the broadening-induced effect might be overestimated in our theory, since the carriers in the absorber are coupling to the contacts with the same strength irrespective of their positions (we therefore can discuss a single parameter τ_{out} for carrier extraction time). On the other hand, it seems to be a general fact irrespective of details of the modeling that fast carrier extraction before thermalization will not be beneficial without using other tricks like those used in hot-carrier solar cells as discussed below.

The reduction of η_{max} in fast extraction regime III in Fig. 11 may be confusing because the hot carrier solar cells that are targeted in this regime can surpass the SQ limit of η^{SQ} theoretically [3–7]. Therefore, we may expect an increase in η_{max} as τ_{out} decreases in regime III. However, this discrepancy is not surprising and can be explained as follows. The differences in the results stem from the differences between the carrier extraction processes. A hot carrier solar cell uses a filter to select the energies of the carriers that pass from the absorber to the electrodes, which can reduce the heat dissipation (thermal losses) in the electrodes. Tailored filtering can increase the output voltage while preventing large output current losses in hot carrier solar cells. However, our simple planar solar cell in Fig. 11 does not use such a filter, and the heat dissipation in the electrodes is therefore not controlled. As already shown
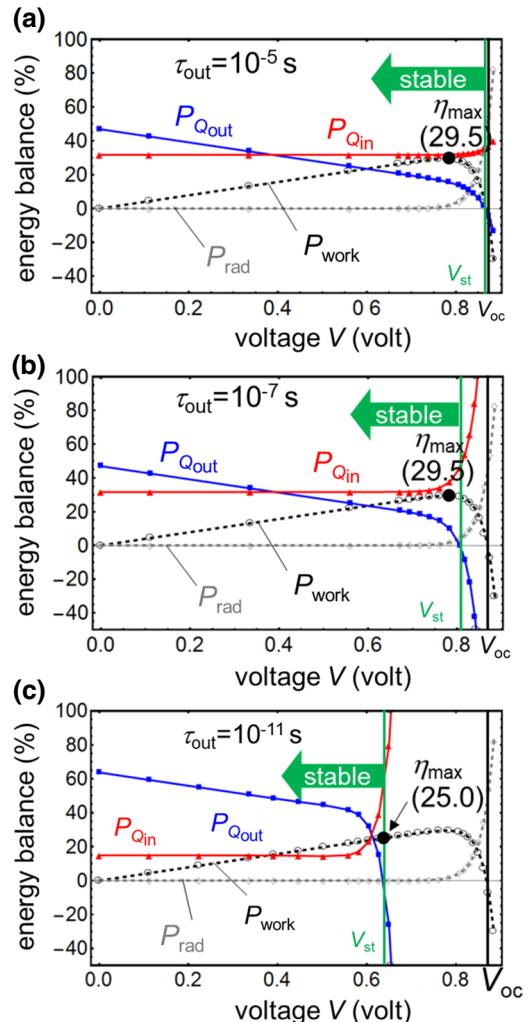

FIG. 17. Energy balance shown as a function of bias voltage V for various carrier extraction times: (a) $\tau_{\text{out}} = 10^{-5}$, (b) 10^{-7}, and (c) 10^{-11} s (100-μm-thick Si under 1-sun-AM0 illumination). For the ideal model with heat-isolated phonon reservoirs shown in Fig. 12(b), the stability condition is given by $P_{Q_{\text{in}}} > 0$ and $P_{Q_{\text{out}}} > 0$, which is fulfilled for $V < V_{\text{st}}$ (green vertical lines). Note that the fraction from transmission loss P_T of the subbandgap light is 21.4 percent (not shown here).

in Fig. 14 and as will be shown in the next subsection (Fig. 17), heat losses, and especially the heat loss in the electrodes, increase in regime III. This results in a strong reduction in η_{max} in our case. These contrasting results support the supposition that, unless a tailored carrier extraction process such as that using energy selection is used, it is difficult for fast carrier extraction before thermalization to be beneficial.

B. Another limiting case: heat-isolated phonon reservoirs

The maximum conversion efficiency η_{max} is also dependent on the phonon environment that surrounds the solar

cell. In this subsection, we focus on solar-cell performance in another limiting case with the heat-isolated phonon reservoirs shown in Fig. 12(b). When exchange of phonons between the absorber and electrode crystals is prevented both directly and indirectly, i.e., when their phonon environments are isolated [e.g., baths 3 and 4 in Fig. 12(b)], $\eta_{\max}$ is significantly reduced from the values obtained for heat-shared reservoirs for a small τ_{out}. Similar results are obtained, irrespective of the value of $\mathcal{CR}$.

Here we explain how these differences occur. In the heat-isolated phonon reservoirs, the stability condition for the solar cell requires $P_{Q_{\text{in}}} > 0$ and $P_{Q_{\text{out}}} > 0$. Otherwise, an additional heat supply must be added to the absorber or the electrodes, which is not suitable for our targeted device. To be more precise, let us consider a situation where $P_{Q_{\text{out}}} < 0$ (as found below) and what will happen next in the device. In this case, the electrodes require heat supply from others for the stable operation. However, supply from the absorber lattice is prohibited in the heat-isolated model. With no heat supply, the lattice temperature of the electrodes, initially at the ambient temperature, will decrease. Then, the cooled electrodes will start to collect heat from the ambient air (e.g., surrounding air) at the higher temperature. Then, the cooled electrodes will cool the ambient air next during the solar-cell operation. Semiconductor devices with similar structure, which cool down the ambient air for the operation, can exist in reality as found in light-emitting diodes (LEDs) (namely, refrigerating LEDs [53–57]). However, solar cells are the devices aimed for long-term stand-alone operation requiring the stability at a long time scale. In our model simulation with heat-isolated reservoirs, we consider the device with $P_{Q_{\text{out}}} < 0$ inevitably requires an additional heat supply for the stable operation.

In Fig. 17, the energy balance is shown as a function of bias voltage V for various carrier extraction times: (a) $\tau_{\text{out}} = 10^{-5}$, (b) 10^{-7}, and (c) 10^{-11} s. To address the stability condition, we plotted the contributions from the heat flow into the absorber $P_{Q_{\text{in}}}$ and into the electrodes $P_{Q_{\text{out}}}$ separately. As shown by the plots, $P_{Q_{\text{out}}}$ decreases with V and changes sign from positive to negative at a point $V = V_{\text{st}}$, whereas $P_{Q_{\text{in}}}$ always remains positive. We call V_{st} the stability boundary here because the stability condition is fulfilled for $V < V_{\text{st}}$.

When the carrier extraction is slow, e.g., when $\tau_{\text{out}} = 10^{-5}$ s in Fig. 17(a), V_{st} is almost the same as V_{oc}. This means that the heat flow direction between absorber and electrodes is the same as the charge flow direction. We consider this to be the normal situation. However, when the extraction becomes faster, as shown in Fig. 17(b) and Fig. 17(c), we find a clear departure of V_{st} from V_{oc}. In this case, we find the regime where $V_{\text{st}} < V < V_{\text{oc}}$, in which $P_{\text{work}} > 0$ but $P_{Q_{\text{out}}} < 0$, i.e., where the heat flow and charge flow directions are different. In this regime, the solar cell generates electric power ($P_{\text{work}} > 0$), but an

external heat supply of no less than $|P_{Q_{\text{out}}}|$ must be additionally provided for the electrodes. Such a device would not provide a solar cell operating in a self-sustained manner using solar illumination alone. In this way, we have evaluated $\eta_{\max}$ to be the maximum conversion efficiency under the stability conditions $0 < V < V_{\text{st}}$. For example, in Fig. 17, $\eta_{\max}$ is 29.5 percent for $\tau_{\text{out}} = 10^{-5}$ and 10^{-7} s, whereas $\eta_{\max}$ is reduced to 25.0 percent for $\tau_{\text{out}} = 10^{-11}$ s.

As already shown in Fig. 14, the sum $P_{Q_{\text{in}}} + P_{Q_{\text{out}}}$ is positive as long as $0 < V < V_{\text{oc}}$. Therefore, if thermally linked, the depleted heat in the electrodes when $V_{\text{st}} < V < V_{\text{oc}}$ can be complemented by the heat inflow into the absorber denoted by $P_{Q_{\text{in}}}$. The ideal limit in such a case with a strong thermal link corresponds to the heat-shared phonon reservoirs that are discussed in Sec. IV A. In real situations where the thermal link strength is moderate (i.e., heat depletion in the electrodes is partially complemented by the absorber via phonon transport), $\eta_{\max}$ will be located between the two ideal cases (the solid and dashed curves in Fig. 11). Because the difference between these two results is large, we propose that $\eta_{\max}$ is sensitive to the phonon transport between the absorber and the electrodes (in either direct or indirect ways) in the fast carrier extraction regime.

V. CONCLUSION AND FUTURE PROSPECTS

We formulate a nonequilibrium theory for solar cells that includes microscopic descriptions of the carrier thermalization and extraction processes. This theory extends the Shockley-Queisser theory to nonequilibrium parameter regimes where the detailed balance cannot be applied. The theory provides detailed information about the solar cells, including nonequilibrium carrier distribution functions with the chemical potentials that are higher than those in the electrodes, and the energy balance (including output work, radiation losses, transmission losses, and heat dissipation in the absorber and the electrodes), which will provide a precise understanding of the loss mechanisms in various solar-cell types for a wide range of parameters.

Using the nonequilibrium theory, we define three different regimes in terms of their carrier extraction time that are bounded using two time scales: the thermalization time, τ_{ph}, and $\tau_{\text{out}}^{\text{ul}*}$, at which the device characteristics should change. The upper boundary $\tau_{\text{out}}^{\text{ul}*}$ is dependent on the absorber material parameters, and is more strongly dependent on the system parameters, e.g., the absorber thickness and solar light concentration ratio.

Device simulations of simple planar solar cells have shown that the SQ limit is applicable in the normal extraction regime, denoted by regime II ($\tau_{\text{ph}} < \tau_{\text{out}} < \tau_{\text{out}}^{\text{ul}*}$) in Fig. 8. Outside this regime (in regimes I and III), nonequilibrium carrier populations are found in the absorber and the maximum conversion efficiency is significantly

reduced from the SQ limit. While the reductions in $\eta_{\max}$ are similar, the energy-loss mechanisms in the fast and slow extraction regimes are different, which is clearly reflected in their I-V characteristics. The reduction in $\eta_{\max}$ in the fast extraction regime also indicates that unless a tailored carrier extraction procedure such as that based on energy selection is performed, it would be difficult for fast carrier extraction before carrier thermalization to be beneficial. This strong claim is consistent with the fact that hot carrier solar cells require energy selection during their carrier extraction processes in addition to the fast extraction procedure.

The nonequilibrium theory presented here covers only a few basic elements of solar cells and has only been tested in simple planar solar cells. The losses of photogenerated carriers in the absorber in this work are solely due to radiative recombination. Inclusion of nonradiative recombination may change the result, as will be discussed elsewhere. In the carrier extraction process, this paper does not consider energy losses at the junction. A case of this type using ohmic contacts will be studied in future work. Application of the proposed theory to other types of solar cells, e.g., organic solar cells, perovskite solar cells, multijunction solar cells, intermediate-band solar cells, and hot carrier solar cells will also be interesting. The most important and challenging aspect will be to provide feasible proposals for new solar cells using nonequilibrium features by which the SQ limit can be surpassed.

ACKNOWLEDGMENTS

APPENDIX A: MICROSCOPIC DERIVATION: EXTRACTION RATE $R_{E_E}^{E(H),\mathrm{OUT}}$

The relaxation dynamics of a system of interest caused by weak interaction with the environment can be described using a standard approach that is widely used in studies of open quantum systems [58,59]. The carrier extraction rate, $R_{E_{e(h)}}^{e(h),\mathrm{out}}$, is also obtained using a similar approach. First, as shown in Fig. 1, complete solar-cell systems are divided into four parts: the main electron-hole systems in the absorber [carrier system (sys)], the electron and hole reservoirs (baths 1 and 2), and the phonon reservoir (bath 3). Therefore, the noninteracting Hamiltonian for the whole system, H_0, can be given as the sum of four parts, i.e., $H_0 = H_{0,\mathrm{sys}} + H_{0,\mathrm{bath}\,1} + H_{0,\mathrm{bath}\,2} + H_{0,\mathrm{bath}\,3}$, where

$$H_{0,\mathrm{sys}} = \sum_k \left\{ [E_g + E_e(k)]e_k^\dagger e_k + E_h(k)h_k^\dagger h_k \right\}, \quad (A1)$$

$$H_{0,\mathrm{bath}\,1} = \sum_{k'} \epsilon_{k'}^c c_{k'}^\dagger c_{k'}, \quad (A2)$$

$$H_{0,\mathrm{bath}\,2} = \sum_{k'} \epsilon_{k'}^d d_{k'}^\dagger d_{k'}, \quad (A3)$$

$$H_{0,\mathrm{bath}\,3} = \sum_q E_q^{\mathrm{ph}} b_q^\dagger b_q. \quad (A4)$$

Here, e_k and h_k are fermionic annihilation operators that are defined using the anticommutation relations, $[e_k, e_{k'}^\dagger]_+ = [h_k, h_{k'}^\dagger]_+ = \delta_{k,k'}$ ($[X, Y]_+ \equiv XY + YX$), of the electrons and holes in the carrier system (absorber), with momentum k and energies of $E_g + E_e(k)$ and $E_h(k)$, respectively. $c_{k'}$ and $d_{k'}$ represent the fermionic annihilation operators when defined using the anticommutation relations $[c_k, c_{k'}^\dagger]_+ = [d_k, d_{k'}^\dagger]_+ = \delta_{k,k'}$ for the electrons in bath 1 and the holes in bath 2 with momentum k', and energies of $\epsilon_{k'}^c$ and $\epsilon_{k'}^d$, respectively. b_q represents a bosonic annihilation operator, which is defined using the commutation relation $[b_q, b_{q'}^\dagger]_- = \delta_{q,q'}$ ($[X, Y]_- \equiv XY - YX$) for the phonons in bath 3 (the crystal lattice in the absorber) with momentum q and energy E_q^{ph}. Under the assumption of weak carrier system interaction with the environments (bath 1 + bath 2 + bath 3), the density matrix of the whole system ρ can be approximated using a product of the matrices for the subsystems:

$$\rho = \rho_{\mathrm{sys}} \otimes \rho_{\mathrm{bath}\,1} \otimes \rho_{\mathrm{bath}\,2} \otimes \rho_{\mathrm{bath}\,3}. \quad (A5)$$

With this density matrix, the quantum and statistical average for any physical quantity O is given by $\langle O \rangle = \mathrm{Tr}(O\rho)$. Here, the density matrix for the carrier system, denoted by ρ_{sys}, is the matrix of interest and will be determined using the von Neumann equation [59]. Additionally, the density matrices for the environments are assumed to be

$$\rho_{\mathrm{bath}\,1} = \exp\left[-\beta_c(H_{0,\mathrm{bath}\,1} - \mu_c N_c) \right] / Z_{\mathrm{bath}\,1}, \quad (A6)$$

$$\rho_{\mathrm{bath}\,2} = \exp\left\{ -\beta_c[H_{0,\mathrm{bath}\,2} - (-\mu_v)N_d] \right\} / Z_{\mathrm{bath}\,2}, \quad (A7)$$

$$\rho_{\mathrm{bath}\,3} = \exp\left(-\beta_{\mathrm{ph}} H_{0,\mathrm{bath}\,3} \right) / Z_{\mathrm{bath}\,3}, \quad (A8)$$

which represent the matrices in their thermal equilibrium states, e.g., with temperature T_c and electron chemical potential μ_c for bath 1, T_c and hole chemical potential $\mu_h(= -\mu_v)$ for bath 2, and phonon temperature T_{ph} and a chemical potential of zero for bath 3. The βs represent inverse temperatures. $N_c = \sum_{k'} c_{k'}^\dagger c_{k'}$ and $N_d = \sum_{k'} d_{k'}^\dagger d_{k'}$ represent the total numbers of carriers in bath 1 and bath 2, respectively, and the Zs are normalization factors used to

ensure that

$$\text{Tr}(\rho_{\text{bath 1}}) = \text{Tr}(\rho_{\text{bath 2}}) = \text{Tr}(\rho_{\text{bath 3}}) = 1. \quad (A9)$$

Using the density matrix, the distribution functions for the carriers in the absorber are defined as

$$n_k^e = n_{E_e[=E_e(k)]}^e \equiv \langle e_k^\dagger e_k \rangle, \quad (A10)$$

$$n_k^h = n_{E_h[=E_h(k)]}^h \equiv \langle h_k^\dagger h_k \rangle, \quad (A11)$$

while those for the particles in the baths are given by

$$\langle c_{k'}^\dagger c_{k'} \rangle = f_{\mu_c,\beta_c}^F(\epsilon_{k'}^c), \quad (A12)$$

$$\langle d_{k'}^\dagger d_{k'} \rangle = f_{-\mu_v,\beta_c}^F(\epsilon_{k'}^v) \quad (A13)$$

$$\langle b_q^\dagger b_q \rangle = f_{0,\beta_{\text{ph}}}^B(E_q^{\text{ph}}), \quad (A14)$$

where $f_{\mu,\beta}^F(E)\{\equiv 1/[e^{\beta(E-\mu)}+1]\}$ and $f_{\mu,\beta}^B(E)$ $\{\equiv 1/[e^{\beta(E-\mu)}-1]\}$ are the Fermi-Dirac and Bose-Einstein distribution functions, respectively, with inverse temperature β and chemical potential μ.

The electron extraction rate appears as a perturbation expansion to the kinetic motion in the equations for the distribution functions of the second order with respect to the weak interaction between the carrier system and bath 1, $H' = H_{\text{sys−bath 1}}$, whereas the interaction Hamiltonian is given using the form

$$H_{\text{sys−bath 1}} = \sum_{k,k'}[T_{k,k'}^e e_k c_{k'}^\dagger + (T_{k,k'}^e)^* c_{k'} e_k^\dagger]. \quad (A15)$$

The coupling parameter $T_{k,k'}^e$ represents the tunneling amplitude of an electron passing from the absorber through the tunnel barrier to the electron reservoir. Therefore, $T_{k,k'}^e$, is a function of the overlap integral of the wavefunctions in the absorber and the reservoir, i.e., it is a function of k and k', the height and width of the tunnel barrier, and the absorber thickness.

Switching to the interaction picture, where $O_I(t) \equiv e^{i(H_0/\hbar)t}Oe^{-i(H_0/\hbar)t}$, the von Neumann equation for the density matrix is given as

$$\frac{d}{dt}\rho_I(t) = \frac{1}{i\hbar}[H_I'(t), \rho_I(t)]_-, \quad (A16)$$

where

$$H_I'(t) = \sum_{k,k'}[T_{k,k'}^e e_k c_{k'}^\dagger e^{-i(E_g+E_e-\epsilon_{k'}^c)t/\hbar} + \text{h. c.}] \quad (A17)$$

is the interaction Hamiltonian, given by $H'(= H_{\text{sys−bath 1}})$, in the interaction picture. Successive iterations and time

integration of Eq. (A16) gives

$$\frac{d}{dt}\rho_I = \left(\frac{1}{i\hbar}\right)^2 \int_0^\infty \{H_I'(t), [H_I'(t-\tau), \rho_I(t-\tau)]_-\}_- d\tau$$

$$\sim \left(\frac{1}{i\hbar}\right)^2 \int_0^\infty \{H_I'(t), [H_I'(t-\tau), \rho_I(t)]_-\}_- d\tau, \quad (A18)$$

where the initial time contribution from $t = -\infty$ is neglected in the first equation, and a Markov approximation, under the assumption that the main system dynamics are sufficiently slow when compared with the memory time in the environments, is used in the second equation [58,59]. Because we are considering steady-state operation of the solar cells, the Markov approximation can be used safely.

Using Eq. (A18), the extraction rate for an electron with kinetic energy $E_e[= E_e(k)]$ for momentum k is given by

$$-R_{E_e}^{e,\text{out}} = \frac{d}{dt}\langle e_k^\dagger e_k \rangle = \text{Tr}\left[e_k^\dagger e_k \dot{\rho}_I(t)\right]$$

$$= \left(\frac{1}{i\hbar}\right)^2 \int_0^\infty \text{Tr}\left(e_k^\dagger e_k[H_I'(t),\right.$$

$$\left. \{H_I'(t-\tau), \rho_I(t)]_-\}_-\right) d\tau \quad (A19)$$

Using the cyclic property of the trace, where $\text{Tr}(XYZ) = \text{Tr}(ZXY)$, the integrand on the right-hand side of the third equation is given explicitly by

$$\text{Tr}\left\{\left[e_k^\dagger e_k H_I'(t)H_I'(t-\tau) + H_I'(t-\tau)H_I'(t)e_k^\dagger e_k\right.\right.$$

$$\left.\left. - H_I'(t-\tau)e_k^\dagger e_k H_I'(t) - H_I'(t)e_k^\dagger e_k H_I'(t-\tau)\right]\rho_I(t)\right\}. \quad (A20)$$

Considering the assumption in Eq. (A5), the trace for the whole system can be provided by successive partial traces of the subsystems. By retaining only the terms that do not vanish after the trace is taken, Eq. (A20) can be rewritten as

$$\sum_{k'} |T_{k,k'}^e|^2 [e^{i(E_g+E_e-\epsilon_{k'}^c)\tau/\hbar} - e^{-i(E_g+E_e-\epsilon_{k'}^c)\tau/\hbar}]$$

$$\times \text{Tr}\left[(e_k^\dagger e_k e_k^\dagger e_k c_{k'} c_{k'}^\dagger - e_k e_k^\dagger e_k e_k^\dagger c_{k'}^\dagger c_{k'})\rho_I(t)\right]$$

$$= \sum_{k'} |T_{k,k'}^e|^2 [e^{i(E_g+E_e-\epsilon_{k'}^c)\tau/\hbar} - e^{-i(E_g+E_e-\epsilon_{k'}^c)\tau/\hbar}]$$

$$\times \left\{n_{E_e}^e[1 - f_{\mu_c,\beta_c}^F(\epsilon_{k'}^c)] - (1 - n_{E_e}^e)f_{\mu_c,\beta_c}^F(\epsilon_{k'}^c)\right\}, \quad (A21)$$

where math operations like

$$\text{Tr}\left[e_k^\dagger e_k e_k^\dagger e_k c_{k'} c_{k'}^\dagger \rho_I(t)\right]$$

$$= \text{Tr}\left[e_k^\dagger e_k c_{k'} c_{k'}^\dagger \rho_{\text{sys},I}(t) \otimes \rho_{\text{bath 1}} \otimes \rho_{\text{bath 2}} \otimes \rho_{\text{bath 3}}\right]$$

$$= \text{Tr}\left[e_k^\dagger e_k \rho_{\text{sys},I}(t)\right] \times \text{Tr}\left(c_{k'} c_{k'}^\dagger \rho_{\text{bath 1}}\right)$$

$$= n_k^e(t) \times [1 - f_{\mu_c,\beta_c}^F(\epsilon_{k'}^c)], \qquad (A22)$$

are performed in Eq. (A21). In the right-hand side of Eq. (A21), the terms in the bracket proportional to $n^e(1 - f^F)$ and $(1 - n^e)f^F$ represent the rates for extraction from and injection to the absorber, respectively. Thus, the term in Eq. (A21) gives the net extraction rate from the absorber as a whole. By inserting Eq. (A21) into Eq. (A19) and performing the integration with respect to time, we obtain Fermi's golden rule result for the extraction rate,

$$R_{E_e}^{e,\text{out}} = \frac{2\pi}{\hbar} \sum_{k'} |T_{k,k'}^e|^2 \delta(E_g + E_e - \epsilon_{k'}^c)$$

$$\times \left[n_{E_e}^e - f_{\mu_c,\beta_c}^F(E_g + E_e)\right]. \qquad (A23)$$

We therefore derive a simple expression for the extraction rate:

$$R_{E_e}^{e,\text{out}} = \frac{1}{\tau_{\text{out}}^e}\left[n_{E_e}^e - f_{\mu_c,\beta_c}^F(E_g + E_e)\right], \qquad (A24)$$

with extraction time τ_{out}^e that is defined as

$$(\tau_{\text{out}}^e)^{-1} = \frac{2\pi}{\hbar}|T^e(E)|^2 \mathcal{D}_c(E)\bigg|_{E=E_g+E_e}, \qquad (A25)$$

where $\mathcal{D}_c(E)[= \sum_{k'} \delta(E - \epsilon_{k'}^c)]$ is the density of states in bath 1, and

$$|T^e(E)|^2 = \frac{\sum_{k'} |T_{k,k'}^e|^2 \delta(E - \epsilon_{k'}^c)}{\sum_{k'} \delta(E - \epsilon_{k'}^c)}, \qquad (A26)$$

represents the strength of tunneling coupling when averaged over the states in bath 1 at energy E. While τ_{out}^e is dependent on the energy of the carriers, we consider it to be a constant parameter in the following analysis for simplicity. In this sense, the carrier extraction time used here is an effective parameter representative for all the electrons tunneling between the absorber and the electrode.

The same argument is also applicable to the hole extraction rate when using $H' = H_{\text{sys-bath2}} = \sum_{k,k'}(T_{k,k'}^h h_k d_{k'}^\dagger +$

H.c.). We therefore have a similar expression for holes:

$$R_{E_h}^{h,\text{out}} = \frac{1}{\tau_{\text{out}}^h}\left[n_{E_h}^h - f_{-\mu_v,\beta_c}^F(E_h)\right], \qquad (A27)$$

with a hole extraction time of

$$(\tau_{\text{out}}^h)^{-1} = \frac{2\pi}{\hbar} \sum_{k'} |T_{k,k'}^h|^2 \delta(E_h - \epsilon_{k'}^d)$$

$$\equiv \frac{2\pi}{\hbar}|T^h(E)|^2 \mathcal{D}_d(E)\bigg|_{E=E_h}, \qquad (A28)$$

where $|T^h(E)|^2$ is an effective tunneling probability for a hole tunneling from the absorber to bath 2, and $\mathcal{D}_d(E)[= \sum_{k'} \delta(E - \epsilon_{k'}^d)]$ is the density of states in bath 2 at energy E. In the following, we also assume the simplest case, i.e., where $\tau_{\text{out}}^e = \tau_{\text{out}}^h \equiv \tau_{\text{out}}$, which will not limit the generality of the main conclusion. We note here that the description based on the tunnel Hamiltonian given in Eq. (A15) simply neglects the voltage drop at the contact. Ohmic contacts with energy losses at the contacts are outside the scope of this paper.

APPENDIX B: MICROSCOPIC DERIVATION: PHONON SCATTERING RATE $R_{E_E}^{E(H),\text{PHONON}}$

The phonon scattering (thermalization) rate in the rate equation for the microscopic carrier distribution functions, given by $R_{E_{e(h)}}^{e(h),\text{phonon}}$, can be derived using an analysis similar to those presented in Appendix A. In this case, interactions between the carriers and the phonons are considered using the perturbation Hamiltonian $H' = H_{\text{sys-bath3}}$, which is given by

$$H_{\text{sys-bath3}} = \sum_{q,k} g_q^c(b_q + b_{-q}^\dagger)(e_{k+q}^\dagger e_k + \text{H.c.})$$

$$+ \sum_{q,k} g_q^v(b_q + b_{-q}^\dagger)(h_{k+q}^\dagger h_k + \text{H.c.}), \quad (B1)$$

where g_q^c and g_q^v are the electron-phonon coupling constants for the bottom-conduction-band and top-valence-band electrons in the absorber, respectively. The q dependence of the coupling constants is dependent on the types of phonons involved. For an order of magnitude-level estimate of the thermalization rate, the LA phonons that originate from the deformation potential are considered for Si absorbers:

$$g_q^{c(v)} = a_{\text{def},c(v)} \sqrt{\frac{\hbar q}{2\mathcal{V}v_A\rho_A}}, \qquad (B2)$$

where $a_{\text{def},c(v)}$, v_A, and ρ_A are the deformation potential for the conduction (valence) electrons, the phonon velocity,

and the mass density in the absorber, respectively. A realistic estimate requires inclusion of the scattering caused by the other phonon modes, i.e., the transverse acoustic (TA), transverse optical (TO), and LO modes, and the intravalley scattering (within the degenerate bands) [42], based on realistic electron and phonon band structures [41], which is far beyond the scope of this work.

The interaction Hamiltonian in the interaction picture is

$$
\begin{aligned}
H'_I(t) &= \sum_{q,k} \left\{ g^c_q e^\dagger_{k+q} e_k b_q e^{i[E_e(k+q)-E_e(k)-E^{\mathrm{ph}}_q]t/\hbar} + \mathrm{H.c.} \right\} \\
&+ \sum_{q,k} \left\{ g^c_q e^\dagger_{k+q} e_k b^\dagger_{-q} e^{i[E_e(k+q)-E_e(k)+E^{\mathrm{ph}}_q]t/\hbar} + \mathrm{H.c.} \right\} \\
&+ \sum_{q,k} \left\{ g^v_q h^\dagger_{k+q} h_k b_q e^{i[E_h(k+q)-E_h(k)-E^{\mathrm{ph}}_q]t/\hbar} + \mathrm{H.c.} \right\} \\
&+ \sum_{q,k} \left\{ g^v_q h^\dagger_{k+q} h_k b^\dagger_{-q} e^{i[E_h(k+q)-E_h(k)+E^{\mathrm{ph}}_q]t/\hbar} + \mathrm{H.c.} \right\}.
\end{aligned}
$$
(B3)

Insertion of Eq. (B3) into $\mathrm{Tr}[e^\dagger_k e_k \dot{\rho}_I(t)]$ with the second-order Born-Markov approximation given in Eq. (A18) and performing a time integration, we obtain the phonon scattering rates as follows:

$$
\begin{aligned}
R^{e,\mathrm{phonon}}_{E_e} &= \frac{2\pi}{\hbar} \sum_q (g^c_q)^2 \\
&\times \delta[E_e(k)-E_e(k-q)-E^{\mathrm{ph}}_q]\{n^e_k(1-n^e_{k-q}) \\
&\times [f^B_{0,\beta_{\mathrm{ph}}}(E^{\mathrm{ph}}_q)+1] - n^e_{k-q}(1-n^e_k)f^B_{0,\beta_{\mathrm{ph}}}(E^{\mathrm{ph}}_q)\} \\
&- \frac{2\pi}{\hbar} \sum_q (g^c_q)^2 \delta[E_e(k+q)-E_e(k)-E^{\mathrm{ph}}_q] \\
&\times n^e_{k+q}(1-n^e_k)[f^B_{0,\beta_{\mathrm{ph}}}(E^{\mathrm{ph}}_q)+1] \\
&- n^e_k(1-n^e_{k+q})[f^B_{0,\beta_{\mathrm{ph}}}(E^{\mathrm{ph}}_q)],
\end{aligned}
$$
(B4)

$$
\begin{aligned}
R^{h,\mathrm{phonon}}_{E_h} &= \frac{2\pi}{\hbar} \sum_q (g^v_q)^2 \\
&\times \delta[E_h(k)-E_h(k-q)-E^{\mathrm{ph}}_q]\{n^h_k(1-n^h_{k-q}) \\
&\times [f^B_{0,\beta_{\mathrm{ph}}}(E^{\mathrm{ph}}_q)+1] - n^h_{k-q}(1-n^h_k)f^B_{0,\beta_{\mathrm{ph}}}(E^{\mathrm{ph}}_q)\} \\
&- \frac{2\pi}{\hbar} \sum_q (g^v_q)^2 \delta[E_h(k+q)-E_h(k)-E^{\mathrm{ph}}_q] \\
&\times \{n^h_{k+q}(1-n^h_k)[f^B_{0,\beta_{\mathrm{ph}}}(E^{\mathrm{ph}}_q)+1] \\
&- n^h_k(1-n^h_{k+q})f^B_{0,\beta_{\mathrm{ph}}}(E^{\mathrm{ph}}_q)\}.
\end{aligned}
$$
(B5)

Scattering rates in this form are equivalent to those obtained using Fermi's golden rule calculation. The expression above includes a momentum representation of the carrier distribution functions that can be further stated using simpler expressions in the energy representation. First, we transform the q summation into an integration over polar coordinates in the form $\sum_q = \mathcal{V}(2\pi)^3 \int_0^\infty 2\pi |q|^2 d|q| \int_{-1}^1 d(\cos\theta)$, where θ is the angle between k and q. The angular integration is then performed using the dispersion relation $E^{\mathrm{ph}}_q = \hbar v_A |q|$, the coupling constants for LA phonons in Eq. (B2), and

$$
E_{e(h)}(k) - E_{e(h)}(k-q) = \frac{\hbar^2 (2|q||k|\cos\theta - |q|^2)}{2m^*_{e(h)}}, \quad \text{(B6)}
$$

$$
E_{e(h)}(k+q) - E_{e(h)}(k) = \frac{\hbar^2 (2|q||k|\cos\theta + |q|^2)}{2m^*_{e(h)}}. \quad \text{(B7)}
$$

By making a change in the coordinates, where $|q| = \epsilon/(\hbar v_A)$, we finally obtain

$$
\begin{aligned}
R^{e(h),\mathrm{phonon}}_{E_{e(h)}} &= C^{e(h)}_{\mathrm{ph}} \int_0^{\epsilon^{e(h),-}_{\mathrm{cut}}} \frac{\epsilon^2 d\epsilon}{\sqrt{E_{e(h)}}} \{n^{e(h)}_{E_{e(h)}}[1-n^{e(h)}_{E_{e(h)}-\epsilon}] \\
&\times [1+f^B_{0,\beta_{\mathrm{ph}}}(\epsilon)] - n^{e(h)}_{E_{e(h)}-\epsilon}[1-n^{e(h)}_{E_{e(h)}}]f^B_{0,\beta_{\mathrm{ph}}}(\epsilon)\} \\
&- C^{e(h)}_{\mathrm{ph}} \int_0^{\epsilon^{e(h),+}_{\mathrm{cut}}} \frac{\epsilon^2 d\epsilon}{\sqrt{E_{e(h)}}} \{n^{e(h)}_{E_{e(h)}+\epsilon}[1-n^{e(h)}_{E_{e(h)}}] \\
&\times [1+f^B_{0,\beta_{\mathrm{ph}}}(\epsilon)] - n^{e(h)}_{E_{e(h)}}[1-n^{e(h)}_{E_{e(h)}+\epsilon}]f^B_{0,\beta_{\mathrm{ph}}}(\epsilon)\}.
\end{aligned}
$$
(B8)

Terms proportional to $f^B_{0,\beta_{\mathrm{ph}}}(\epsilon)$ and $1+f^B_{0,\beta_{\mathrm{ph}}}(\epsilon)$ represent the scattering rates for phonon absorption and emission, respectively. Here, we newly defined the coefficient $C^{e(h)}_{\mathrm{ph}} \equiv \frac{a^2_{\mathrm{def,c(v)}}\sqrt{m^*_{e(h)}/2}}{4\pi\hbar^4 v_A^4 \rho_A}$ and the $E_{e(h)}$-dependent cutoff energies as follows:

$$
\epsilon^{e(h),-}_{\mathrm{cut}} \equiv \min\{E_{e(h)}, \epsilon^{\mathrm{ph}}_{\mathrm{cut}}, 2v_A[\sqrt{2m^*_{e(h)}E_{e(h)}} - m^*_{e(h)}v_A]\},
$$
(B9)

$$
\epsilon^{e(h),+}_{\mathrm{cut}} \equiv \min\left\{\epsilon^{\mathrm{ph}}_{\mathrm{cut}}, 2v_A\left[\sqrt{2m^*_{e(h)}E_{e(h)}} + m^*_{e(h)}v_A\right]\right\},
$$
(B10)

where $\epsilon^{\mathrm{ph}}_{\mathrm{cut}}$ is the Debye cutoff energy for the LA phonons (approximately 50 meV for Si). The $E_{e(h)}$ dependences in Eqs. (B9) and (B10) stem from the condition that the arguments in the delta functions in Eqs. (B4) and (B5) are zero, i.e., from the requirements for energy and momentum conservation during the carrier-phonon scattering processes. A situation also occurs in which the cutoff energy $\epsilon^{e(h),-}_{\mathrm{cut}}$ becomes negative. This occurs when

$\sqrt{2m^*_{e(h)}E_{e(h)}} - m^*_{e(h)}v_A < 0$ for small $E_{e(h)}$, i.e., when $E_{e(h)} < \frac{1}{2}m^*_{e(h)}v_A^2 \equiv E^{PB}_{e(h)}$. In this case, carriers with $E_{e(h)} < E^{PB}_{e(h)}$ cannot lose energy via phonon emissions (i.e., carrier cooling does not occur), even at the zero temperature of the lattice ($T_{\rm ph} = 0$), which is prohibited by the conservation law. However, this effect, which is called the phonon bottleneck effect, is normally negligible because the threshold energy $E^{PB}_{e(h)}$, known as the phonon bottleneck energy, is very low (e.g., $v_A = 10^4$ m/s, $m^*_e/m_e = 1.08$, and $m^*_h/m_e = 0.55$ give $E^{PB}_e = 0.307$ meV and $E^{PB}_h = 0.156$ meV in the model for Si). We have already implicitly assumed that $E_{e(h)} > E^{PB}_{e(h)}$ in Eq. (B8) (which sets $\epsilon^{e(h),-}_{\rm cut} > 0$ and the lower domain boundary of the latter integration to zero).

APPENDIX C: INCLUSION OF SPECTRAL BROADENING

Using the Gaussian line function $\mathcal{A}_\Gamma(x)$, expressions for the generation and loss rates in the rate equation that has been derived thus far are modified as follows, where the modification becomes important when $\tau_{\rm out} \ll \tau^{e(h)}_{\rm ph}$.

For the generation rate $R^{e(h),sun}_{E_{e(h)}}$—because the Sun's spectrum is much broader than the broadening of the states, $k_B T_S \gg \Gamma$, we can neglect the effects of broadening on $R^{e(h),\rm sun}_{E_{e(h)}}$. We therefore use Eqs. (7) and (8) for direct gap semiconductors and Eq. (30) and (31) for direct gap semiconductors.

For the radiative recombination loss rate $R^{e(h),rad}_{E_{e(h)}}$— inclusion of the spectral broadening modifies the density of states of the carriers. This effect replaces $\mathcal{D}_{e(h)}(E)$ with $\tilde{\mathcal{D}}_{e(h)}(E)$ in the analysis that is presented in Sec. II B [particularly in Eqs. (15), (16), (25), and (26)], where

$$\tilde{\mathcal{D}}_{e(h)}(E) \equiv \left[\mathcal{D}_{e(h)} * \mathcal{A}_\Gamma\right](E)$$
$$= \int_0^\infty \mathcal{D}_{e(h)}(E')\mathcal{A}_\Gamma(E - E')dE', \qquad \text{(C1)}$$

is the density of states of the carriers convolved using the spectral function. For example, the denominator in both Eqs. (25) and (26) can be modified as follows:

$$\int_{-\infty}^\infty \tilde{\mathcal{D}}_e(E')\tilde{\mathcal{D}}_h(\Delta E - E')dE'$$
$$= \int_{-\infty}^\infty dE' \int_0^\infty dE_e \int_0^\infty dE_h \mathcal{D}_e(E_e)\mathcal{A}_\Gamma(E' - E_e)$$
$$\times \mathcal{D}_h(E_h)\mathcal{A}_\Gamma(\Delta E - E' - E_h)$$
$$= \int_0^\infty dE_e \int_0^\infty dE_h \mathcal{D}_e(E_e)\mathcal{D}_h(E_h)$$
$$\times \mathcal{A}_{\sqrt{2}\Gamma}(\Delta E - E_e - E_h). \qquad \text{(C2)}$$

In the last equation, we used a general property of the convolution of Gaussian functions:

$$\mathcal{A}_{\Gamma_1} * \mathcal{A}_{\Gamma_2}(E) \equiv \int_{-\infty}^\infty dE' \mathcal{A}_{\Gamma_1}(E')\mathcal{A}_{\Gamma_2}(E - E')$$
$$= \mathcal{A}_{\sqrt{\Gamma_1^2 + \Gamma_2^2}}(E). \qquad \text{(C3)}$$

A similar modification is made to the numerator in Eqs. (25) and (26). As a result, the recombination loss rates for the indirect transition are given by

$$R^{e,\rm rad}_{E_e} = \frac{1}{w} \times \frac{c}{2\pi^2}\left(\frac{1}{\hbar c}\right)^3 \times \int_0^\infty dE\, E^2$$
$$\times \frac{\int_0^\infty \mathcal{D}_h(E_h')n^e_{E_e}n^h_{E_h'}\mathcal{A}_{\sqrt{2}\Gamma}(\Delta E - E_e - E_h')dE_h'}{\iint \mathcal{D}_e(E_e')\mathcal{D}_h(E_h')\mathcal{A}_{\sqrt{2}\Gamma}(\Delta E - E_e' - E_h')dE_e'dE_h'}, \qquad \text{(C4)}$$

$$R^{h,\rm rad}_{E_h} = \frac{1}{w} \times \frac{c}{2\pi^2}\left(\frac{1}{\hbar c}\right)^3 \times \int_0^\infty dE\, E^2$$
$$\frac{\int_0^\infty \mathcal{D}_e(E_e')n^e_{E_e'}n^h_{E_h}\mathcal{A}_{\sqrt{2}\Gamma}(\Delta E - E_e' - E_h)dE_e'}{\iint \mathcal{D}_e(E_e')\mathcal{D}_h(E_h')\mathcal{A}_{\sqrt{2}\Gamma}(\Delta E - E_e' - E_h')dE_e'dE_h'}, \qquad \text{(C5)}$$

for the electrons and holes, respectively (where the approximation $1 - n^e_{E_e} - n^h_{E_h} \approx 1$ is used). The above expressions can be simplified further by introducing the dimensionless functions $\Phi(x)$ and $\Theta(x,y)$:

$$\Phi(x) \equiv \int_0^\infty \frac{ds}{\sqrt{\pi}}s^2 e^{-(s-x)^2}$$
$$= \frac{xe^{-x^2}}{2\sqrt{\pi}} + \frac{(1 + 2x^2)[1 + \text{erf}(x)]}{4}, \qquad \text{(C6)}$$

$$\Theta(x,y) \equiv \int_{-x}^\infty \frac{(s + x)^2}{\Phi(s)} \times \frac{e^{-(s-y)^2}}{\sqrt{\pi}}ds, \qquad \text{(C7)}$$

where $\text{erf}(x)$ is the Gaussian error function and $\Psi(x)$ has the following asymptotic forms:

$$\Phi(x \gg 1) = x^2, \quad \Phi(x \ll -1) = \frac{e^{-x^2}}{4\sqrt{\pi}|x|^3}. \qquad \text{(C8)}$$

Using these functions, Eqs. (C4) and (C5) can be rewritten as

$$R^{e,\rm rad}_{E_e} = \frac{8}{\pi d_e}\left(\frac{c/w}{2\pi^2}\right)\left(\frac{1}{\hbar c}\right)^3 n^e_{E_e}$$
$$\times \int_0^\infty \sqrt{E_h}\Theta\left(\frac{E_g}{\sqrt{2}\Gamma}, \frac{E_e + E_h}{\sqrt{2}\Gamma}\right)n^h_{E_h}dE_h, \qquad \text{(C9)}$$

$$R_{E_h}^{h,\mathrm{rad}} = \frac{8}{\pi d_h} \left(\frac{c/w}{2\pi^2}\right) \left(\frac{1}{\hbar c}\right)^3 n_{E_h}^h$$

$$\times \int_0^\infty \sqrt{E_e} \Theta \left(\frac{E_g}{\sqrt{2}\Gamma}, \frac{E_e + E_h}{\sqrt{2}\Gamma}\right) n_{E_e}^e dE_e. \quad (C10)$$

Within the limit from $\Gamma \to +0$, we find that $\Theta \to (E_g + E_e + E_h)^2/(E_e + E_h)^2$ in the integrands, which reproduces the original expressions of Eqs. (30) and (31). Equations (C9) and (C10), when derived in this way, are the explicit forms of the radiation loss rates for indirect gap semiconductor absorbers.

A similar analysis is also applied to direct gap semiconductor absorbers. We find that the expressions in Eq. (32) and (33) are modified by the broadening effect as follows:

$$R_{E_e}^{e,\mathrm{rad}} = \frac{c}{2\pi^2 w} \left(\frac{1}{\hbar c}\right)^3 \frac{\left(1 + \frac{m_e^*}{m_h^*}\right)}{d_e \sqrt{E_e}}$$

$$\times \int_0^\infty E^2 \frac{\sqrt{E_{eh}} \mathcal{A}_{\sqrt{2}\Gamma}(\Delta E - E_{eh}) n_{E_e}^e n_{E_h}^h}{\int_0^\infty \sqrt{E'_{eh}} \mathcal{A}_{\sqrt{2}\Gamma}(\Delta E - E'_{eh}) dE'_{eh}} dE, \quad (C11)$$

$$R_{E_e}^{h,\mathrm{rad}} = \frac{c}{2\pi^2 w} \left(\frac{1}{\hbar c}\right)^3 \frac{\left(1 + \frac{m_h^*}{m_e^*}\right)}{d_h \sqrt{E_h}}$$

$$\times \int_0^\infty E^2 \frac{\sqrt{E_{eh}} \mathcal{A}_{\sqrt{2}\Gamma}(\Delta E - E_{eh}) n_{E_e}^e n_{E_h}^h}{\int_0^\infty \sqrt{E'_{eh}} \mathcal{A}_{\sqrt{2}\Gamma}(\Delta E - E'_{eh}) dE'_{eh}} dE, \quad (C12)$$

where we used the approximation $1 - n_{E_e}^e - n_{E_h}^h \approx 1$. Here, $\Delta E \equiv E - E_g$ and $m_e^* E_e = m_h^* E_h$ for direct gap semiconductors, and $E_{eh} \equiv E_e + E_h$.

For the carrier extraction rate $R_{E_{e(h)}}^{e(h),out}$—inclusion of the broadening effect in this term is straightforward. The incoming particle number rates from the electrodes into the absorber are modified because the single-particle states have a spectral width. After modification, we obtain

$$R_{E_e}^{e,\mathrm{out}} = \frac{1}{\tau_{\mathrm{out}}} \left[n_{E_e}^e - \tilde{f}_{\mu_c, \beta_c}^F (E_g + E_e) \right], \quad (C13)$$

$$R_{E_h}^{h,\mathrm{out}} = \frac{1}{\tau_{\mathrm{out}}} \left[n_{E_h}^h - \tilde{f}_{-\mu_v, \beta_c}^F (E_h) \right], \quad (C14)$$

where we assume that $\tau_{\mathrm{out}}^{e(h)} = \tau_{\mathrm{out}}$, and the Fermi-Dirac distribution convolved with the lineshape function is given by

$$\tilde{f}_{\mu,\beta}^F (E) = (f_{\mu,\beta}^F * \mathcal{A}_\Gamma)(E)$$

$$= \int_{-\infty}^\infty f_{\mu,\beta}^F (E') \mathcal{A}_\Gamma (E - E') dE'. \quad (C15)$$

For the phonon scattering rate: $R_{E_{e(h)}}^{e(h),phonon}$—inclusion of the broadening effect replaces the δ functions in Eqs. (B4)

and (B5) with the convolved lineshape functions as follows:

$$\delta[E_{e(h)}(k) - E_{e(h)}(k - q) - E_q^{\mathrm{ph}}]$$

$$\to \mathcal{A}_{\sqrt{2}\Gamma}[E_{e(h)}(k) - E_{e(h)}(k - q) - E_q^{\mathrm{ph}}],$$

$$\left\{ = \int_{-\infty}^\infty dE_1 \int_{-\infty}^\infty dE_2 \, \delta(E_1 - E_2 - E_q^{\mathrm{ph}}) \right.$$

$$\left. \times \mathcal{A}_\Gamma [E_1 - E_{e(h)}(k)] \mathcal{A}_\Gamma [E_2 - E_{e(h)}(k - q)] \right\}$$

$$\delta[E_{e(h)}(k + q) - E_{e(h)}(k) - E_q^{\mathrm{ph}}] \quad (C16)$$

$$\to \mathcal{A}_{\sqrt{2}\Gamma}[E_{e(h)}(k + q) - E_{e(h)}(k) - E_q^{\mathrm{ph}}]. \quad (C17)$$

After the replacement, we can transform the q summation into an integration over polar coordinates, and the angular integration can finally be performed, as done in Sec. II D. The final result is

$$R_{E_{e(h)}}^{e(h),\mathrm{phonon}} = \frac{C_{\mathrm{ph}}^{e(h)}}{\sqrt{E_{e(h)}}} \int_0^{\epsilon_{\mathrm{cut}}^{\mathrm{ph}}} \epsilon^2 d\epsilon \int_{E_-}^{E_+} dE'$$

$$\mathcal{A}_{\sqrt{2}\Gamma}[E_{e(h)} - E' - \epsilon]\{n_{E_{e(h)}}^{e(h)}[1 - n_{E'}^{e(h)}]$$

$$\times [1 + f_{0,\beta_{\mathrm{ph}}}^B (\epsilon)] - n_{E'}^{e(h)}[1 - n_{E_{e(h)}}^{e(h)}] f_{0,\beta_{\mathrm{ph}}}^B (\epsilon)\}$$

$$- \frac{C_{\mathrm{ph}}^{e(h)}}{\sqrt{E_{e(h)}}} \int_0^{\epsilon_{\mathrm{cut}}^{\mathrm{ph}}} \epsilon^2 d\epsilon \int_{E_-}^{E_+} dE'$$

$$\mathcal{A}_{\sqrt{2}\Gamma}[E_{e(h)} - E' + \epsilon]\{n_{E'}^{e(h)}[1 - n_{E_{e(h)}}^{e(h)}]$$

$$\times [1 + f_{0,\beta_{\mathrm{ph}}}^B (\epsilon)] - n_{E_{e(h)}}^{e(h)}[1 - n_{E'}^{e(h)}] f_{0,\beta_{\mathrm{ph}}}^B (\epsilon)\}, \quad (C18)$$

where we defined $E_\pm$ as

$$E_\pm \equiv \left(\sqrt{E_{e(h)}} \pm \epsilon \sqrt{\frac{1}{2m_{e(h)}^* v_A^2}} \right)^2 \geq 0. \quad (C19)$$

Within the limit from $\Gamma \to +0$ in Eq. (C18), the Gaussian function $\mathcal{A}_{\sqrt{2}\Gamma}$ becomes δ functions. The terms that remain after integration of E' should come from the poles $E' = E_{e(h)} \pm \epsilon$, which are located in the interval $E_- < E'(= E_{e(h)} \pm \epsilon) < E_+$. In this way, Eq. (C18) safely reproduces Eq. (B8) when $\Gamma = +0$. Here, we assume again that $E_{e(h)} > E_{e(h)}^{PB}$, i.e., that the phonon bottleneck effect is neglected as it is in Eq. (B8).

The reason for adoption of the Gaussian lineshape—As mentioned earlier in this subsection, we use a Gaussian lineshape for the microscopic states, despite the fact that it cannot be derived naturally for an ideal model without statistical fluctuations. This lineshape is adopted for the following technical reason. We derive rate equations

for the microscopic distribution functions of the carriers in both direct and indirect gap semiconductor absorbers. In the derivation for the indirect gap semiconductors, we introduce a probability density of $p^{e(h)}[E_{e(h)}]$ in Eq. (9) and use it to obtain the generation rate $R_{E_{e(h)}}^{e(h),\text{sun}}$ and the recombination loss rate $R_{E_{e(h)}}^{e(h),\text{rad}}$. The factor $\int_0^{\Delta E} \mathcal{D}_e(E')\mathcal{D}_h(\Delta E - E')dE'$ that is found in the denominator in each of Eqs. (10), (25), and (26) can all be traced back to the same normalization factor in the definition of $p^{e(h)}[E_{e(h)}]$ in Eq. (9), i.e., the number of possible combinations of all electron-hole pairs with E_e and E_h that can emit a photon of energy E. If the spectral broadening of the microscopic states is included, the normalization factor should then be modified by replacing $\mathcal{D}_{e(h)}(E)$ with $\tilde{\mathcal{D}}_{e(h)}(E)$ [as defined in Eq. (C1)], as shown in Eq. (C2). No problems arise with the mathematics here if Gaussian lineshape function $\mathcal{A}_\Gamma(x)$ is used for the lineshape. However, if we use the Lorentzian lineshape function,

$$\mathcal{A}_\Gamma^L(x) \equiv \frac{1}{\pi}\frac{\Gamma}{x^2 + \Gamma^2}, \tag{C20}$$

the situation changes. Using a similar analysis, the normalization factor is calculated to be

$$\int_{-\infty}^{\infty} \tilde{\mathcal{D}}_e(E')\tilde{\mathcal{D}}_h(\Delta E - E')dE'$$
$$= \int_{-\infty}^{\infty} dE' \int_0^{\infty} dE_e \int_0^{\infty} dE_h \mathcal{D}_e(E_e)\mathcal{A}_\Gamma^L(E' - E_e)$$
$$\times \mathcal{D}_h(E_h)\mathcal{A}_\Gamma^L(\Delta E - E' - E_h)$$
$$= \int_0^{\infty} dE_e \int_0^{\infty} dE_h \mathcal{D}_e(E_e)\mathcal{D}_h(E_h)$$
$$\times \mathcal{A}_{2\Gamma}^L(\Delta E - E_e - E_h). \tag{C21}$$

In the last equation, we use a general property of the convolution of Lorentzian functions:

$$\mathcal{A}_{\Gamma_1}^L * \mathcal{A}_{\Gamma_2}^L(E) \equiv \int_{-\infty}^{\infty} dE' \mathcal{A}_{\Gamma_1}^L(E')\mathcal{A}_{\Gamma_2}^L(E - E')$$
$$= \mathcal{A}_{\Gamma_1+\Gamma_2}^L(E). \tag{C22}$$

The integration can also be performed by changing the integration variable to $E_{eh} \equiv E_e + E_h$ and E_h, which results in the following divergence:

$$\int_{-\infty}^{\infty} \tilde{\mathcal{D}}_e(E')\tilde{\mathcal{D}}_h(\Delta E - E')dE'$$
$$\propto \int_0^{\infty} dE_{eh} \int_0^{E_{eh}} dE_h \sqrt{E_h(E_{eh} - E_h)}\mathcal{A}_{2\Gamma}^L(\Delta E - E_{eh})$$

$$= \frac{\pi}{8}\int_0^{\infty} E_{eh}^2 \mathcal{A}_{2\Gamma}^L(\Delta E - E_{eh})dE_{eh}$$
$$\propto \int_0^{\infty} \frac{E_{eh}^2}{E_{eh}^2 + (2\Gamma)^2}dE_{eh} = +\infty. \tag{C23}$$

This divergence represents a clear artifact that is derives from the simplification of our model of the semiconductor carriers. We adopt an effective two-band model with infinite bandwidths for carriers. Because of these infinite bandwidths, there is no upper domain bound for integration over E_{eh} in Eq. (C23). This prevents us from defining the probability measure for $p^{e(h)}[E_{e(h)}]$ and our formulation thus fails when we use the Lorentzian lineshape function and the infinite bandwidths for the carriers. Of course, this problem can be avoided by introducing an effective bandwidth parameter that should exist naturally. However, the introduction of an additional bandwidth parameter can then reduce the benefits of our simple two-band model with the infinite bandwidths. The final results may also depend on the bandwidth parameter, the definition of which remains unclear. For these reasons, we use the Gaussian lineshape for the spectral function, not having encountered such an artifact, and thus benefit greatly from use of our simplified model. In realistic devices, the semiconductor absorbers are not ideally prepared with structural imperfections to cause statistical fluctuations. As a result, their spectral lineshapes will be more or less Gaussian-like, at least in the tails (which could also be Voigt functions). Even when the Lorentzian lineshape is used in the infinite bandwidth model, this divergence problem does not occur for direct gap semiconductors. Despite the above discussion on possible changes in the formulation, we still expect that the selection of the lineshape functions will not strongly affect the result or the main conclusion of this paper.

———

[1] W. Shockley and H. J. Queisser, Detailed balance limit of efficiency of p-n junction solar cells, J. Appl. Phys. **32**, 510 (1961).

[2] A. Richter, M. Hermle, and S. W. Glunz, Reassessment of the limiting efficiency for crystalline silicon solar cells, IEEE J. Photovoltaics **3**, 1184 (2013).

[3] R. T. Ross and A. J. Nozik, Efficiency of hot-carrier solar energy converters, J. Appl. Phys. **53**, 3813 (1982).

[4] P. Würfel, Solar energy conversion with hot electrons from impact ionisation, Sol. Energy Mater. Sol. Cells **46**, 43 (1997).

[5] Y. Takeda, T. Motohiro, D. König, P. Aliberti, Y. Feng, S. Shrestha, and G. Conibeer, Practical factors lowering conversion efficiency of hot carrier solar cells, Appl. Phys. Exp. **3**, 104301 (2010).

[6] Y. Takeda, A. Ichiki, Y. Kusano, N. Sugimoto, and T. Motohiro, Resonant tunneling diodes as energy-selective contacts used in hot-carrier solar cells, J. Appl. Phys. **118**, 124510 (2015).

[7] D. Suchet, Z. Jehl, Y. Okada, and J-F. Guillemoles, Influence of Hot-Carrier Extraction from a Photovoltaic Absorber: An Evaporative Approach, Phys. Rev. Appl. **8,** 034030 (2017).

[8] M. A. Green, Y. Hishikawa, W. Warta, E. D. Dunlop, D. H. Levi, J. Hohl-Ebinger, and A. W. Ho-Baillie, Solar cell efficiency tables (version 50), Prog. Photovoltaics **25,** 668 (2017).

[9] P. C. Martin and J. Schwinger, Theory of many-particle systems. I, Phys. Rev. **115,** 1342 (1959).

[10] G. Baym and Leo P. Kadanoff, Conservation Laws and Correlation Functions, Phys. Rev. **124,** 287 (1961).

[11] L. V. Keldysh, Diagram technique for nonequilibrium processes, Sov. Phys.—JETP **20,** 1018 (1965).

[12] J. Rammer and H. Smith, Quantum field-theoretical methods in transport theory of metals, Rev. Mod. Phys. **58,** 323 (1986).

[13] S. Datta, *Electronic Transport in Mesoscopic Systems* (Cambridge University Press, Cambridge, 1995).

[14] S. Steiger, R. G. Veprek, and B. Witzigmann, in *Proceedings of the 13th International Workshop on Computational Electronics, IWCE 2009, Beijing, China* (IEEE 2009).

[15] K. Henneberger and H. Haug, Nonlinear optics and transport in laser-excited semiconductors, Phys. Rev. B **38,** 9759 (1988).

[16] S.-C. Lee and A. Wacker, Nonequilibrium Green's function theory for transport and gain properties of quantum cascade structures, Phys. Rev. B **66,** 245314 (2002).

[17] M. H. Szymańska, J. Keeling, and P. B. Littlewood, Nonequilibrium Quantum Condensation in an Incoherently Pumped Dissipative System, Phys. Rev. Lett. **96,** 230602 (2006).

[18] M. Yamaguchi, K. Kamide, R. Nii, T. Ogawa, and Y. Yamamoto, Second Thresholds in BEC-BCS-Laser Crossover of Exciton-Polariton Systems, Phys. Rev. Lett. **111,** 026404 (2013).

[19] U. Aeberhard, Quantum-kinetic theory of photocurrent generation via direct and phonon-mediated optical transitions, Phys. Rev. B **84,** 035454 (2011).

[20] U. Aeberhard, Theory and simulation of quantum photovoltaic devices based on the nonequilibrium Green's function formalism, J. Comp. Electronics **10,** 394 (2011).

[21] N. Cavassilas, F. Michelini, and M. Bescond, Modeling of nanoscale solar cells: The Green's function formalism, J. Renewable Sustainable Energy **6,** 011203 (2014).

[22] U. Aeberhard and U. Rau, Microscopic Perspective on Photovoltaic Reciprocity in Ultrathin Solar Cells, Phys. Rev. Lett. **118,** 247702 (2017).

[23] U. Rau, Reciprocity relation between photovoltaic quantum efficiency and electroluminescent emission of solar cells, Phys. Rev. B **76,** 085303 (2007).

[24] T. Kirchartz and U. Rau, Electroluminescence analysis of high efficiency Cu(In,Ga)Se2 solar cells, J. Appl. Phys. **102,** 104510 (2007).

[25] M. Bernardi, D. Vigil-Fowler, J. Lischner, J. B. Neaton, and S. G. Louie, *Ab Initio* Study of Hot Carriers in the First Picosecond after Sunlight Absorption in Silicon, Phys. Rev. Lett. **112,** 257402 (2014).

[26] U. Würfel, A. Cuevas, and P. Würfel, Charge Carrier Separation in Solar Cells, IEEE J. Photovoltaics, **5,** 461 (2015).

[27] P. Würfel and U. Würfel, *Physics of Solar Cells: From Basic Principles to Advanced Concepts* (Wiley-VCH, Weinheim, 2016), 3rd ed.

[28] P. Würfel, The chemical potential of radiation, J. Phys. C: Solid State Phys. **15,** 3967 (1982).

[29] The photonic density of states could be modified near the surface in the presence of light-trapping textures, whose effect will be small inside the bulk and is simply neglected in our analysis.

[30] C. W. Tang, Two-layer organic photovoltaic cell, Appl. Phys. Lett. **48,** 183 (1986).

[31] G. Yu, J. Gao, J. C. Hummelen, F. Wudl, and A. J. Heeger, Polymer Photovoltaic Cells: Enhanced Efficiencies via a Network of Internal Donor-Acceptor Heterojunctions, Science **270,** 1789 (1995).

[32] B. O'Regan and M. Gratzel, A low-cost, high-efficiency solar cell based on dye-sensitized colloidal TiO$_2$ films, Nature **353,** 737 (1991).

[33] A. Kojima, K. Teshima, Y. Shirai, and T. Miyasaka, Organometal Halide Perovskites as Visible-Light Sensitizers for Photovoltaic Cells, J. Am. Chem. Soc. **131,** 6050 (2009).

[34] J. Frenkel, On the Transformation of light into Heat in Solids. I, Phys. Rev. **37,** 17 (1931).

[35] M. Fox, *Optical Properties of Solids* (Oxford University Press, New York, 2010), 2nd ed., Chap. 4

[36] Y. Tanaka, Y. Noguchi, K. Oda, Y. Nakayama, J. Takahashi, H. Tokairin, and H. Ishii, Evaluation of internal potential distribution and carrier extraction properties of organic solar cells through Kelvin probe and time-of-flight measurements, J. Appl. Phys. **116,** 114503 (2014).

[37] V. M. LeCorre, A. R. Chatri, N. Y. Doumon, and L. J. A. Koster, Charge Carrier Extraction in Organic Solar Cells Governed by Steady-State Mobilities, Adv. Energy Mater. **7,** 1701138 (2017).

[38] N. Cavassilas, C. Gelly, F. Michelini, and M. Bescond, Reflective Barrier Optimization in Ultrathin Single-Junction GaAs Solar Cell, IEEE J. Photovoltaics **5,** 1621 (2015).

[39] U. Aeberhard, Impact of built-in fields and contact configuration on the characteristics of ultra-thin GaAs solar cells, Appl. Phys. Lett. **109,** 033906 (2016).

[40] U. Aeberhard, Quantum-kinetic perspective on photovoltaic device operation in nanostructure-based solar cells, J. Mat. Res. **33,** 373 (2018).

[41] P. Y. Yu and M. Cardona, *Fundamentals of Semiconductors: Physics and Material Properties* (Springer, New York, 2005), 3rd ed.

[42] T. Suzuki and R. Shimano, Cooling dynamics of photoexcited carriers in Si studied using optical pump and terahertz probe spectroscopy, Phys. Rev. B **83,** 085207 (2011).

[43] J. R. Goldman and J. A. Prybyla, Ultrafast Dynamics of Laser-Excited Electron Distributions in Silicon, Phys. Rev. Lett. **72,** 1364 (1994).

[44] A. J. Sabbah and D. M. Riffe, Femtosecond pump-probe reflectivity study of silicon carrier dynamics, Phys. Rev. B **66,** 165217 (2002).

[45] M. Green, *Third Generation Photovoltaics: Advanced Solar Energy Conversion* (Springer-Verlag, Berlin, Heidelberg, 2003).

[46] S. Chen, L. Zhu, M. Yoshita, T. Mochizuki, C. Kim, H. Akiyama, M. Imaizumi, and Y. Kanemitsu, Thorough subcells diagnosis in a multi-junction solar cell via absolute electroluminescence-efficiency measurements, Sci. Rep. **5,** 7836 (2014).

[47] E. Yablonovitch, Statistical ray optics, J. Opt. Soc. Am. **72,** 899 (1982).

[48] J.-K. Yu, S. Mitrovic, D. Tham, J. Varghese, and J. R. Heath, Reduction of thermal conductivity in phononic nanomesh structures, Nat. Nanotechnol. **5,** 718 (2010).

[49] P. E. Hopkins, C. M. Reinke, M. F. Su, R. H. Olsson, E. A. Shaner, Z. C. Leseman, J. R. Serrano, L. M. Phinney, and I. El-Kady, Reduction in the Thermal Conductivity of Single Crystalline Silicon by Phononic Crystal Patterning, Nano Lett. **11,** 107 (2011).

[50] M. G. A. Bernard and G. Duraffourg, Laser Conditions in Semiconductors, Phys. Stat. Solidi B **1,** 699 (1961).

[51] G. J. Conibeer, D. König, M. A. Green, and J. F. Guillemoles, Slowing of carrier cooling in hot carrier solar cells, Thin Solid Films **516,** 6948 (2008).

[52] A. Berbezier and U. Aeberhard, Impact of Nanostructure Configuration on the Photovoltaic Performance of Quantum-Dot Arrays, Phys. Rev. Appl. **4,** 044008 (2015).

[53] J. Xue, Z. Li, and R. J. Ram, Irreversible Thermodynamic Bound for the Efficiency of Light-Emitting Diodes, Phys. Rev. Appl. **8,** 014017 (2017).

[54] J. Tauc, The share of thermal energy taken from the surroundings in the electro-luminescent energy radiated from a p-n junction, Czech. J. Phys. **7,** 275 (1957).

[55] G. C. Dousmanis, C. W. Mueller, H. Nelson, and K. G. Petzinger, Evidence of refrigerating action by means of photon emission in semiconductor diodes, Phys. Rev. **133,** A316 (1964).

[56] P. Berdahl, Radiant refrigeration by semiconductor diodes, J. Appl. Phys. **58,** 1369 (1985).

[57] P. Santhanam, D. J Gray Jr., and R. J. Ram, Thermoelectrically Pumped Light-Emitting Diodes Operating above Unity Efficiency, Phys. Rev. Lett. **108,** 097403 (2012).

[58] H. J. Carmichael, *Statistical Methods in Quantum Optics 1: Master Equations and Fokker-Planck Equations* (Springer, New York, 2002), 2nd ed.

[59] H. P. Breuer and F. Petruccione, *The Theory of Open Quantum Systems* (Oxford University Press, New York, 2002).